

Review

Towards the Application of Purely Inorganic Icosahedral Boron Clusters in Emerging Nanomedicine

Francesc Teixidor, Rosario Núñez *  and Clara Viñas * 

Institut de Ciència de Materials de Barcelona, ICMA-B-CSIC, 08193 Bellaterra, Spain; teixidor@icmab.es

* Correspondence: rosario@icmab.es (R.N.); clara@icmab.es (C.V.)

Abstract: Traditionally, drugs were obtained by extraction from medicinal plants, but more recently also by organic synthesis. Today, medicinal chemistry continues to focus on organic compounds and the majority of commercially available drugs are organic molecules, which can incorporate nitrogen, oxygen, and halogens, as well as carbon and hydrogen. Aromatic organic compounds that play important roles in biochemistry find numerous applications ranging from drug delivery to nanotechnology or biomarkers. We achieved a major accomplishment by demonstrating experimentally/theoretically that boranes, carboranes, as well as metallabis(dicarbollides), exhibit global 3D aromaticity. Based on the stability–aromaticity relationship, as well as on the progress made in the synthesis of derivatized clusters, we have opened up new applications of boron icosahedral clusters as key components in the field of novel healthcare materials. In this brief review, we present the results obtained at the Laboratory of Inorganic Materials and Catalysis (LMI) of the Institut de Ciència de Materials de Barcelona (ICMAB-CSIC) with icosahedral boron clusters. These 3D geometric shape clusters, the semi-metallic nature of boron and the presence of *exo*-cluster hydrogen atoms that can interact with biomolecules through non-covalent hydrogen and dihydrogen bonds, play a key role in endowing these compounds with unique properties in largely unexplored (bio)materials.

Keywords: carboranes; metallabis(dicarbollide); BNCT; proton therapy; PBFR; COSAN; FESAN; PET; SPECT; antimicrobial; luminescence; bioimaging; photodynamic therapy (PDT)



Citation: Teixidor, F.; Núñez, R.; Viñas, C. Towards the Application of Purely Inorganic Icosahedral Boron Clusters in Emerging Nanomedicine. *Molecules* **2023**, *28*, 4449. <https://doi.org/10.3390/molecules28114449>

Academic Editor: Radosław Podsiadły

Received: 27 April 2023

Revised: 21 May 2023

Accepted: 24 May 2023

Published: 30 May 2023



Copyright: © 2023 by the authors. Licensee MDPI, Basel, Switzerland. This article is an open access article distributed under the terms and conditions of the Creative Commons Attribution (CC BY) license (<https://creativecommons.org/licenses/by/4.0/>).

1. Introduction

Boron was isolated in Penzance (Cornwall, England) in 1808 by the English chemist Humphry Davy [1], but boron as an element was identified by Jöns Jakob Berzelius in 1824 [2]. Boron is extracted as borate salts of different cations from minerals (Kaliborite, Karlite, Kernita and Kurnakovite, among others) [3,4]. Turkey (deposits existing in Kırka, Emet, Bigadiç, and Kestelek) has the largest world boron reserves, followed by the United States (“Death Valley” desert in California) and Russia at the second position [5], being Turkey the major country in boron production from 2010 to 2022 [6].

Borax ($\text{Na}_2\text{B}_4\text{O}_7 \cdot 10\text{H}_2\text{O}$) was one of the first minerals to be exchanged in the times of the Ancient World. In the Egypt of the pharaohs, the deceased were embalmed with mummification salts, being those containing borate the most reliable for preservation. Boric acid (H_3BO_3), which was produced from borax by the Dutch chemist William Homberg in 1702, has been widely used for topical administration since the 18th century due to its strong bactericidal and fungicidal activity [7].

Boron, which is located to the left of carbon on the periodic table, possesses and forms stable compounds with a wide variety of elements. Natural boron is composed of two stable isotopes ^{10}B and ^{11}B , the latter of which make up about 80% of natural boron. Boron, like carbon, can bond with itself, forming B-B bonds that give rise to boranes and heteroboranes (being the most known carboranes and metallacarboranes). These boron clusters form 3D aromatic [8–10], polyhedral structures with triangular faces in which the bonds that hold the cluster together are tricentric bonds with two electrons (3c-2e).

William Lipscomb received the Nobel Prize in Chemistry in 1976 for his studies on the 3c-2e bonding of borane structures [11]. These 3D molecular structures of boron clusters possess extraordinary chemical, biological, thermal, and photochemical stability that make them have unique applications in (nano)materials not possible with other elements, including carbon [12–17].

The traditional use of organic chemistry as the basis for all aspects of contemporary biomedical chemistry has provided truly miraculous results. Nowadays, most commercial drugs are purely organic molecules, but nitrogen, oxygen, phosphorus, sulfur, and halogens, all neighbors of carbon to the right, are part of a wide variety of the active principles of medicines. In the middle of the 20th century [18–21], the first investigations of boron compounds for their use in medicine were directed mainly towards the treatment of cancer by the therapy called BNCT (Boron Neutron Capture Therapy), but currently, a vibrant and growing research is being developed to employ boron-containing compounds in medicinal chemistry and chemical biology [22–33].

This mini-review focuses on the large research activity of the Inorganic Materials and Catalysis Laboratory (LMI) at the Institut de Ciència de Materials de Barcelona (ICMAB-CSIC) [34] with icosahedral boron clusters, which due to their geometric shape and the semi-metal nature of boron provide these compounds with unique properties in (bio)materials largely unexplored.

2. Characteristics of Icosahedral Neutral Carboranes and Anionic Metallabis(Dicarbollides)

2.1. Icosahedral Closo-Borane and Heteroborane Clusters

Figure 1 shows the inorganic icosahedral *closo*-dodecaborate ($[B_{10}H_{12}]^{2-}$), the dicarbocloso-dodecaborane (*closo* $C_2B_{10}H_{12}$), which exists in three isomeric forms that are named based on the positioning of the two CH vertices: 1,2- or *ortho*-, 1,7- or *meta*-, and 1,12- or *para*-carborane and, the sandwich metallabis(dicarbollides) $[M(C_2B_9H_{11})_2]^-$ ($M = Co^{3+}$, Fe^{3+}). Five different conformations can be found in the metallabis(dicarbollides): *cisoid-1*, *gauche-1*, *transoid*, *gauche-2* and *cisoid-2*. However, *cisoid-1* and *cisoid-2*, as well as *gauche-1* and *gauche-2*, are equivalent in the non-substituted or symmetrically disubstituted clusters [35].

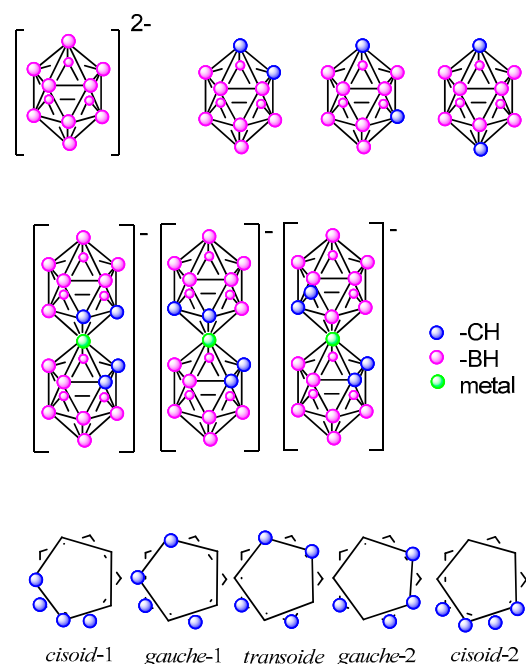


Figure 1. Representation of icosahedral borane, carboranes at the top as well as metallabis(dicarbollides) with the schematic representations of the different conformers of the most known metallabis(*o*-dicarbollide) in the middle and at the bottom, respectively.

Teixidor and Viñas believed that one of the main reasons for the lack of knowledge and poor application of these boron compounds is the lack of synthetic processes for their functionalization. Without these processes, the chemistry of boron is marginalized when its possibilities are enormous, and in many cases, complementary to the organic chemistry compounds.

2.2. Towards the Derivatization of the Icosahedral Boron Clusters

The neutral icosahedral *closo* $C_2B_{10}H_{12}$ carboranes have the potential for the incorporation of a large number of substituents at its 12 vertices (2 C-H and 10 B-H). The reactivity of the B-H vertices depends on the distance of each B-H vertex to the C-H ones. Most reactions that occur at the boron vertices do not affect the carbon vertices, and vice versa. Consequently, *o*-carborane offers the possibility to develop chemistry of neutral *closo*-carboranes at the C vertices, at the B vertices, as well as in both C and B vertices (Figure 2) [35].

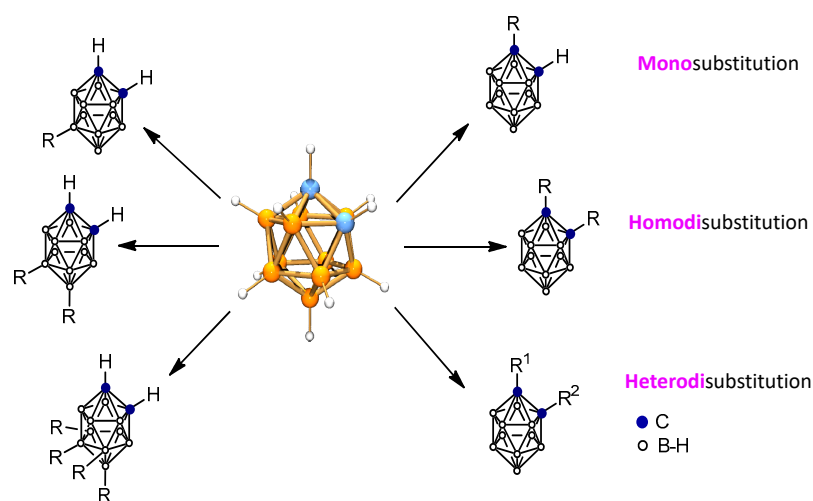


Figure 2. Schematic representation of some substituted *closo ortho*-carboranes at the B vertices (left), at the C vertices (right). Blue circles represent the C atoms, while orange ones the B atoms and white ones are the B atoms or B-H vertices (H atoms omitted for clarity).

Since 1982, Teixidor and Viñas have put emphasis on improving protocols of syntheses because their main objective was the application of icosahedral boron clusters [36], and clusters' derivatization was a necessary and key step to proceed on their use in (bio)materials [37]. Recently, several reviews summarizing the different synthetic procedures to achieve the substitution at the cluster vertices of the icosahedral boron clusters appeared [38–47].

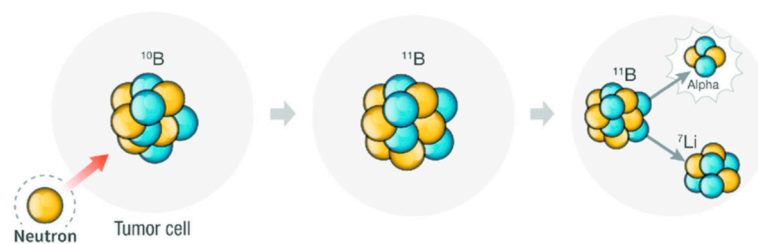
3. Focusing on the Synthesis of Icosahedral Neutral Carborane and Anionic Metallabis(Dicarbollide) Derivatives for Medicinal Application

Teixidor and Viñas group carried out remarkable work in the synthesis of icosahedral carborane and metallacarborane derivatives as well as in their characterization with the objective of finding their application in different fields.

Endo and co-workers, based on the similarities between the phenyl group and the carborane cluster, pioneered the design of new drugs by substituting phenyl groups in compounds with known biological activity with icosahedral carborane groups [48–53]. The concept of 3D aromaticity has already been applied in boron cluster chemistry to relate the limited number of valence electrons in the clusters to their stability [54,55]. Recently [8–10], the 3D global aromaticity of the icosahedral boranes, carboranes, and cobaltabis(dicarbollides) was related to the more familiar 2D aromaticity abiding by Hückel's rule, indicating that both were two sides of the same coin. Then, in 2014 [7], grounded on the relationship between stability and aromaticity, new perspectives for applying icosahedral boron clusters

as key components in the field of new biomaterials for healthcare were opened by Teixidor and Viñas group. The highlight is the development of potentiometric sensors for the detection of drugs [56–59], biosensors [60], and X-ray contrast agents for highly radiopaque vertebroplasty cement [61], among others.

Special emphasis is given to fostering advances in the application of boron compounds for the Boron Neutron Capture Therapy (BNCT) treatment of cancer due to the inherent property of the boron element itself (with 20% of ^{10}B). ^{10}B has a large neutron capture section opening up the application of icosahedral boron clusters to the treatment of cancer by the BNCT reaction between a thermal neutron and ^{10}B resulting in the generation of an α particle and ^7Li nucleus (Scheme 1). Additionally, the 3D aromatic icosahedral boron clusters offer the possibility of holding twelve substituents covering the entire 3D space.



Scheme 1. Representation of the Boron Neutron Capture Therapy reaction (BNCT). Blue circles represents protons while yellow ones neutrons.

The twelve vertices of the cluster can be functionalized, and these small molecules can be converted into multifunctional scaffolds by themselves (Figure 3) [62–65] or bonded to inhibitors of kinases receptor molecules (Figure 4) [66–69] or in anchoring onto structures of nanocarriers (dendrimers [28,70], polymers [14], nanoparticles [36,71–75]) leading to payloads with high boron density (Figure 3). The objective was to synthesize anionic and water-soluble high-boron-containing molecules, which can incorporate in their scaffold either inhibitors of enzymes receptor (Figure 4) [66–69] and/or metal cores (Figure 5) for their use as multifunctional nanocarriers able to act as anticancer drugs by multi-therapy treatment [73–77].

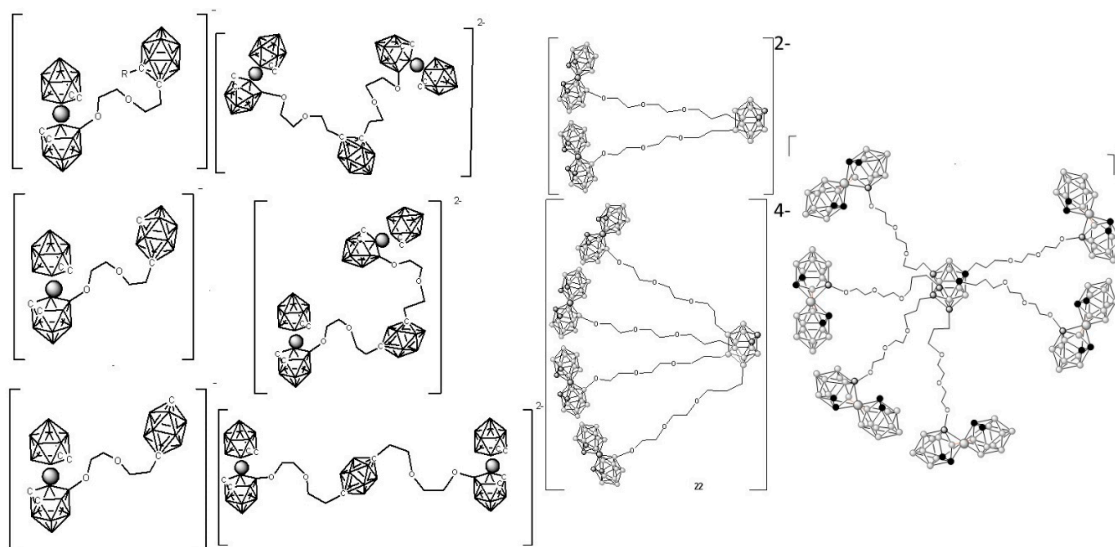


Figure 3. Neutral carborane clusters (*ortho*-, *meta*-, and *para*-) can be functionalized at B, at C, or at both C and B vertices to achieve water-soluble polyanionic high boron content molecules [62–65].

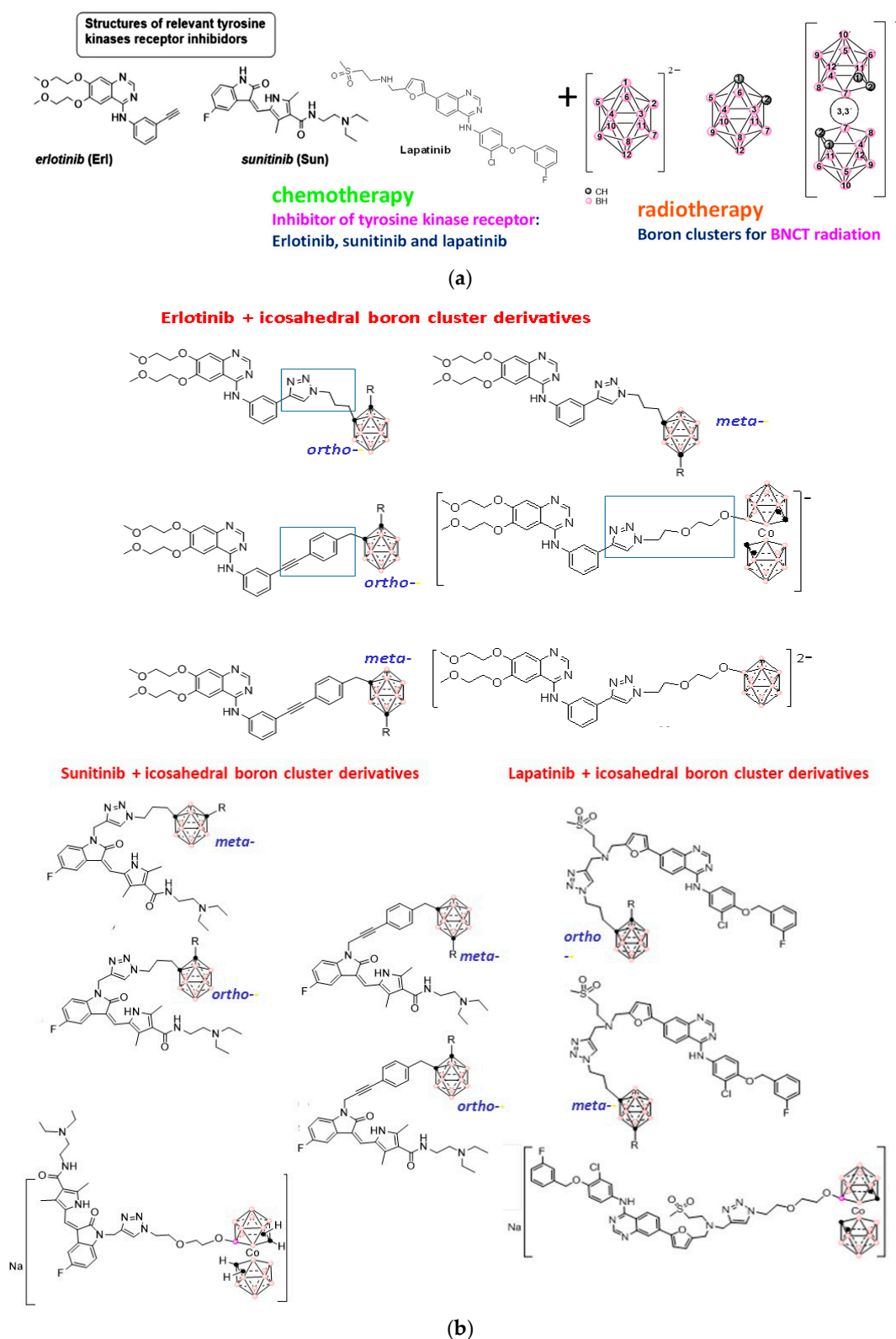


Figure 4. (a) Schematic representation of the two components (inhibitors of kinases receptor + icosahedral boron clusters) of the designed hybrid molecules with potential dual action. (b) The newly synthesized neutral and anionic boron clusters, which contain quinazoline molecules with potential dual action (chemotherapy + radiotherapy) result in significant clinical benefits [66–68]. The black circles represent C atoms or C_C-H vertices, the pink circles represent B-H vertices and the purple ones Boron atoms.

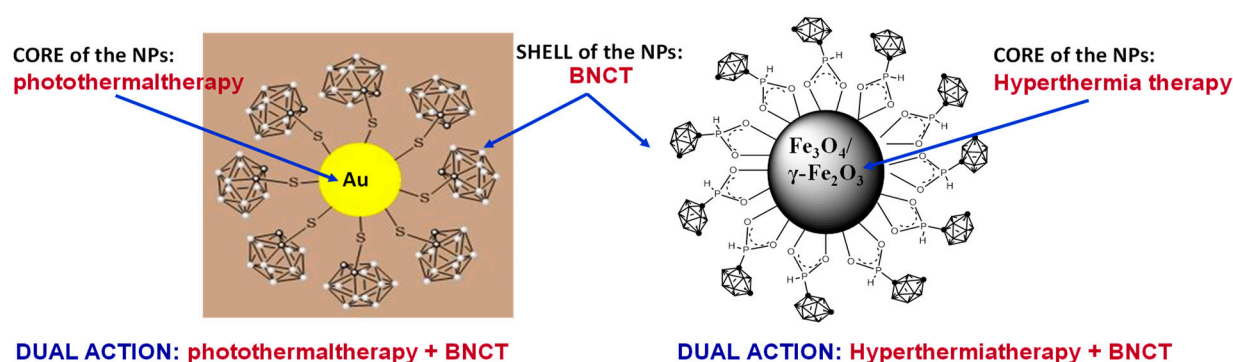


Figure 5. Neutral carboranes onto nanoparticles (gold NPs and magnetic NPs) as vehicles for cancer treatment [71,74]. Both families offer the possibility of dual action (photothermal therapy + BNCT or hyperthermal therapy + BNCT), which may result in significant clinical benefits [73].

4. Testing the Icosahedral Neutral Carboranes and Anionic Metallabis(Dicarbollides) in BNCT Cancer Treatment

4.1. Boron Neutron Capture Therapy

Regarding carboranes for BNCT, the research has focused on the development of new multifunctional hybrid (carboranyl + anilinoquinazolines) nanocarriers [66,67] and carborane-magnetic nanoparticles [73]. These (bio)materials exhibit desirable in vitro antitumor activities against preclinical rat glioblastoma F98, colorectal HT29, glioblastoma A172 cancer cell lines, and human brain endothelial hCMEC/D3 cell line.

Importantly, thermal neutrons irradiation in BNCT for 15 min reduced by 2.5 the number of cultured A172 glioblastoma cells after the treatment with carborane-magnetic nanoparticles (Figure 6a) and the systemic administration of carborane-magnetic nanoparticles in mice was well tolerated with no major signs of toxicity. The dual treatment by combining tyrosine kinase inhibition and BNCT irradiation for minutes on HT-29 cells after incubation with carboranyl + anilinoquinazoline hybrids provided better outcomes than *p*-Boronophenylalanine (BPA) [68]. The attractive profile of developed hybrids makes them interesting agents for combined therapy (Figure 6b).

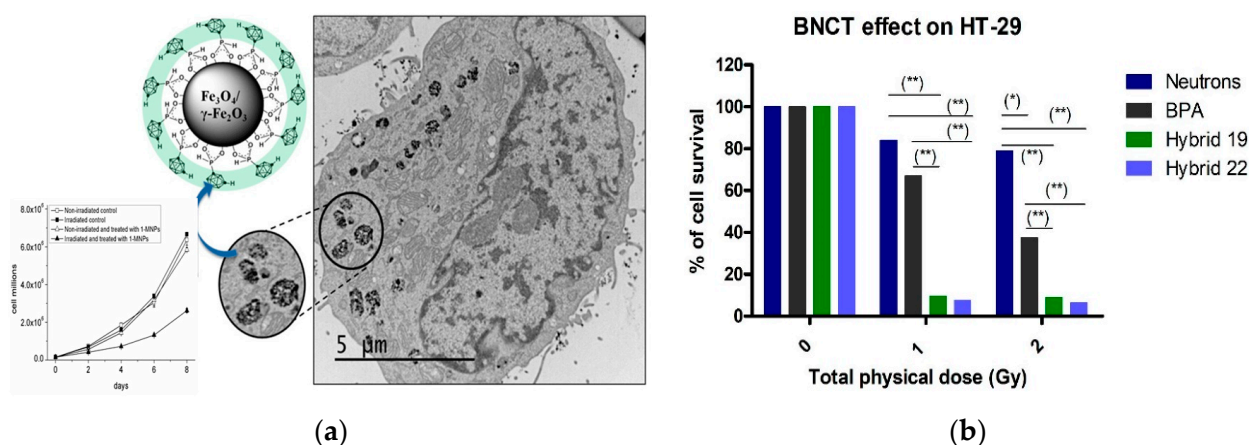


Figure 6. (a) CryoTEM image of glioblastoma A172 cancer cell after carborane-magnetic nanoparticles uptake and proliferation curves of A172 cells re-plated one day after BNCT treatment. BNCT studies were carried out by incubating A172 cells for 24 h with carborane-magnetic nanoparticles (20 $\mu\text{g}/\text{mL}$ boron). The amount of internalized boron measured by ICP-MS was $133 \pm 25 \mu\text{g}/\text{g}$, corresponding to a ^{10}B concentration of $26 \pm 5 \mu\text{g}/\text{g}$ [73]. (b) Effect on HT-29-cell survival without or with hybrids or BPA treatment post-neutron-irradiation (1 and 2 Gy). Compounds were studied at doses equivalent to 10.0 ppm of ^{10}B for 1 h of incubation. (*) $p < 0.05$; (**) $p < 0.01$. Reproduced from Ref. [61] with permission from Wiley & Sons.

4.2. Metallabis(Dicarbollides) Chemical and Physico-Chemical Properties and Cytotoxicity

Regarding the icosahedral metallacarboranes, the anionic metallabis(dicarbollides), $[3,3\text{-M}(1,2\text{-C}_2\text{B}_9\text{H}_{11})_2]^-$, (abbreviated as $[o\text{-COSAN}]^-$ and $[o\text{-FESAN}]^-$ for $\text{M} = \text{Co}$, Fe , respectively), which are inert to biochemical reactions, have attracted much attention in biology [35]. The 3D aromatic $\text{Na}[o\text{-COSAN}]$ forms hydrogen and dihydrogen bonds that participate in its self-assembling, water solubility, and aggregates' formation [76]. The $\text{Na}[o\text{-COSAN}]$ possesses the ability to readily cross cell membranes (Figure 7a) [77–79], is not cytotoxic against mammalian cells (HEK 293, HeLa, THP-1, 3T3), *D. discoideum* amoeba cells, and bacteria (*E. coli* and *Klebsiella*), but is cytostatic, and cells recover following its removal [79]. Furthermore, our studies on glioma-initiating cells (GIC7 and PG88) also supported $\text{Na}[o\text{-COSAN}]$ cytostatic properties when cells were morphologically recovered 43 h after washing off the compound and increasing in the G2/M subpopulation. Additionally, the study showed that mesenchymal PG88 cells that are more resistant than proneural GIC7 cells to conventional radiotherapy have a lower EC_{50} $\text{Na}[o\text{-COSAN}]$ and a higher uptake of the compound compared to GIC7 cells, suggesting a new resource to fight against resistant glioblastoma cells [80].

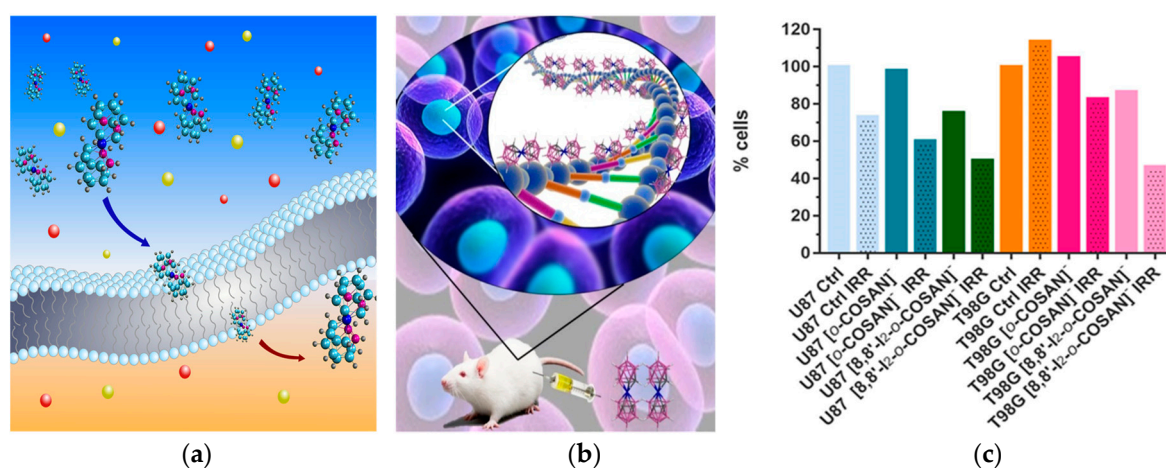


Figure 7. Schematic representation of (a) the $[o\text{-COSAN}]^-$ ability to readily cross cell membranes [65] and (b) $[o\text{-COSAN}]^-$ interaction with DNA [71]. (c) Percentage of viable U87 and T98G cells 24 h after neutron irradiation.

4.3. Synchrotron-Based Fourier-Transform Infrared Micro-Spectroscopy (SR-FTIRM) Studies

Having performed experiments in a round-bottom flask on a chemical scale, which showed that $[o\text{-COSAN}]^-$ and some of its halogenated derivatives interact with biomolecules (amino acids [56,57], proteins [81,82], *ds*-DNA [60,83] (Figure 7b) and glucose [84]), we wanted to go a step ahead by observing these interactions in vitro experiments by using SR-FTIRM. The round-bottom flask changed to a cell, and the solutions to the cell's physiological components. The first chemical scale studies between $[o\text{-COSAN}]^-$ anions and the biomolecules were done individually for each type, whereas the cell study incorporates the effect of all biomolecules interacting simultaneously. This study meant a step ahead to understand and detect that this anion modifies biomolecules (proteins, DNA, and lipids) and concentrates in the cell nucleus after their cellular uptake [68]. The small $\text{Na}[o\text{-COSAN}]$ molecule, localized close to the cell's nucleus, induces proteins' conformational changes and spectral changes of the DNA region (Figure 7b) in both GIC cell lines, similar to the changes induced by other metal-based compounds like cisplatin that disrupt the double helix base pairing, suggesting that $\text{Na}[o\text{-COSAN}]$ is a promising agent for BNCT of glioblastoma.

Consequently, in vitro tests in U87 and T98G cells conclude that the amount of ^{10}B inside the cells is enough for BNCT irradiation. BNCT becomes more effective on T98G after their incubation with $\text{Na}[8,8'\text{-I}_2\text{-}o\text{-COSAN}]$, whereas no apparent cell-killing effect was observed for untreated cells.

All this led to the following conclusions: These small molecules, particularly $[8,8'-I_2-o-COSAN]^-$, are serious candidates for BNCT now that the facilities of accelerator-based neutron sources are more accessible, providing an alternative treatment for resistant glioblastoma (Figure 7c) [85].

Then, *in vivo* experiments with $Na[o-COSAN]$ and $Na[8,8'-I_2-o-COSAN]$ were performed on *Caenorhabditis elegans* (*C. elegans*) at the L4-stage and their embryos. LD50 values for both cobaltabis(dicarbollides) in L4 *C. elegans* were found to be close to the IC₅₀ determined for T98G *in vitro* after 72 h (Figure 8) [86].

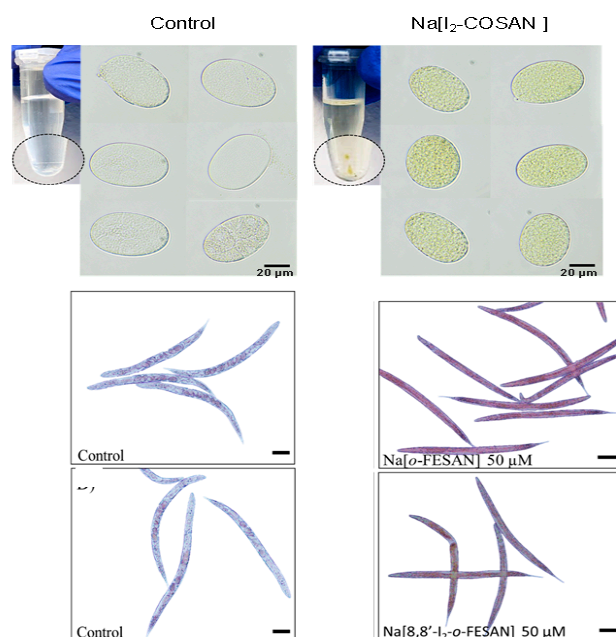


Figure 8. Optical microscopy images of *C. elegans*. (**Top**): The embryos and, (**bottom**): At the L4-stage before (control) and after incubation with $Na[8,8'-I_2-o-COSAN]$ 200 μM [86].

Finally, *in vivo* evaluation in mammalian mice models were run trying to understand the ability of $[o-COSAN]^-$ to target the tumor cells, as well as to cross the blood–brain barrier. After intravenous administration, biodistribution studies of $Na[o-COSAN]$ in BALB/c CrSlc mice (female, 5 weeks old) were run. Anionic $[o-COSAN]^-$ was distributed into many organs but mainly accumulated in the reticuloendothelial system (RES), including liver and spleen (Figure 9) [83].

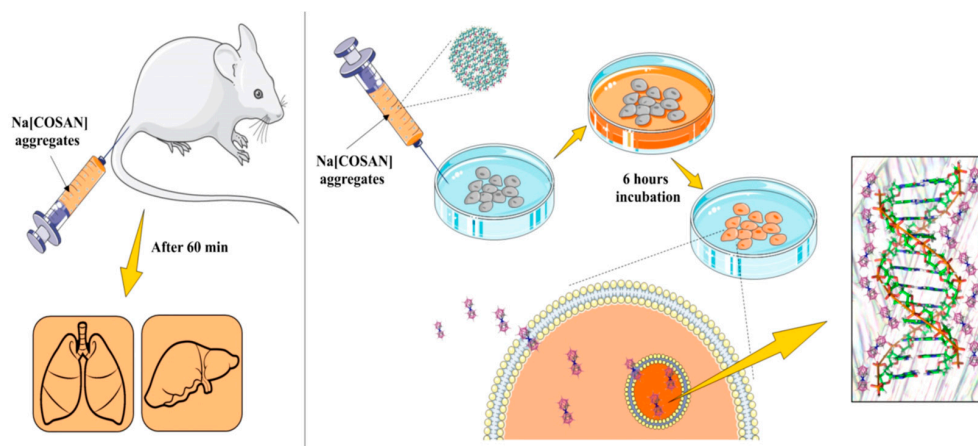


Figure 9. Schematic representation of the *in vitro* (**right**) and *in vivo* (**left**) studies of $Na[o-COSAN]$ [85].

4.4. Contrast Agents

Furthermore, Na[8-I-*o*-COSAN] can be labeled with contrast agents, such as ^{124}I and ^{125}I , for in vivo markers by positron emission tomography (PET) and single photon emission computed tomography (SPECT) nuclear imaging techniques making these clusters very good scaffolds as theranostic agents (Figure 10) [87].

Using Positron Emission Tomography (PET-CT) with ^{124}I

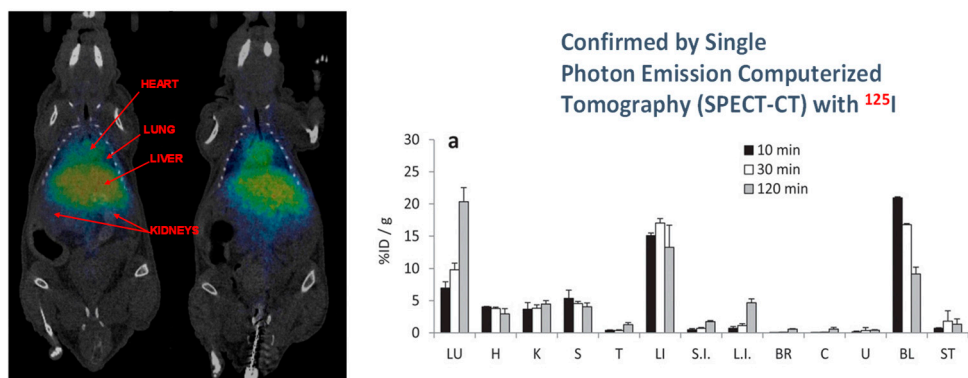
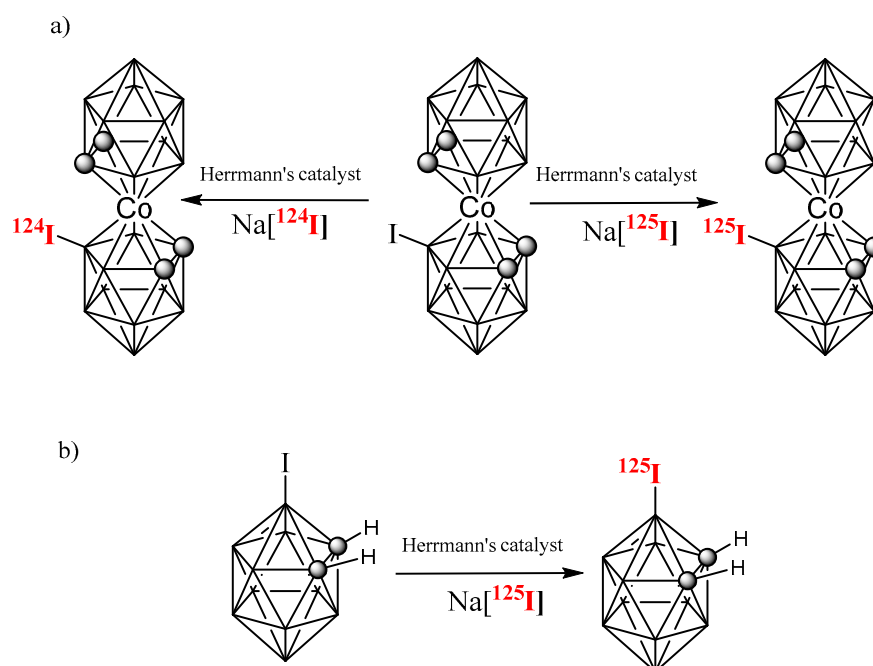


Figure 10. Imaging experiments by in vivo PET-CT and SPECT-CT with Na[8-I-*o*-COSAN] after nuclear interchange of I natural by ^{124}I and ^{125}I , respectively. Reproduced from Ref. [85]. with permission from the Royal Society of Chemistry.

The synthesis of these unprecedented radiolabeling Na[8-I-*o*-COSAN] anionic derivatives with either ^{125}I (gamma emitter) or ^{124}I (positron emitter) was achieved via palladium-catalyzed isotopic exchange reaction (Scheme 2a) following our previously reported synthesis of ^{125}I carborane derivatives (2-I-*p*-, 3-I-*o*-, 9-I-*o*-, 9-I-*m*-carborane, 1-phenyl-3-I-*o*-carborane, and 1,2-diphenyl-3-I-*o*-carborane) with some modifications (Scheme 2b) [87].



Scheme 2. Isotopic exchange: (a) Between [^{124}I]iodide, [^{125}I]iodide, and the anionic [8-I-*o*-COSAN] $^-$ cluster, (b) between [^{125}I]iodide and the neutral 3-iodo-*o*-carborane cluster by using Herrmann's catalyst (the organopalladium compound made by reaction of tris(*o*-tolyl)phosphine with palladium(II) acetate).

Recently, the sodium salt of the anionic $[o\text{-FESAN}]^-$ isotopically 100% ^{57}Fe was synthesized with the objective of treating glioblastoma cancer with $\text{Na}[3,3'\text{-}^{57}\text{Fe}(1,2\text{-C}_2\text{B}_9\text{H}_{11})_2]$ because the compound offers the possibility of dual-action (radiation + drug combinations) to improve clinical benefits and reduce healthy tissues toxicity. After $[o\text{-}^{57}\text{FESAN}]^-$ uptake by U87 glioblastoma cells, $[o\text{-}^{57}\text{FESAN}]^-$ was found to be within the cells with 29% of its uptake in the nuclear fraction, which is a particularly desirable target because the nucleus is the cell control center in which DNA and transcription machinery reside. The multi-therapies activity through irradiation with potential for glioblastoma treatment by the Mossbauer effect of $[3,3'\text{-}^{57}\text{Fe}(1,2\text{-C}_2\text{B}_9\text{H}_{11})_2]^-$ was demonstrated (Figure 11) [88].

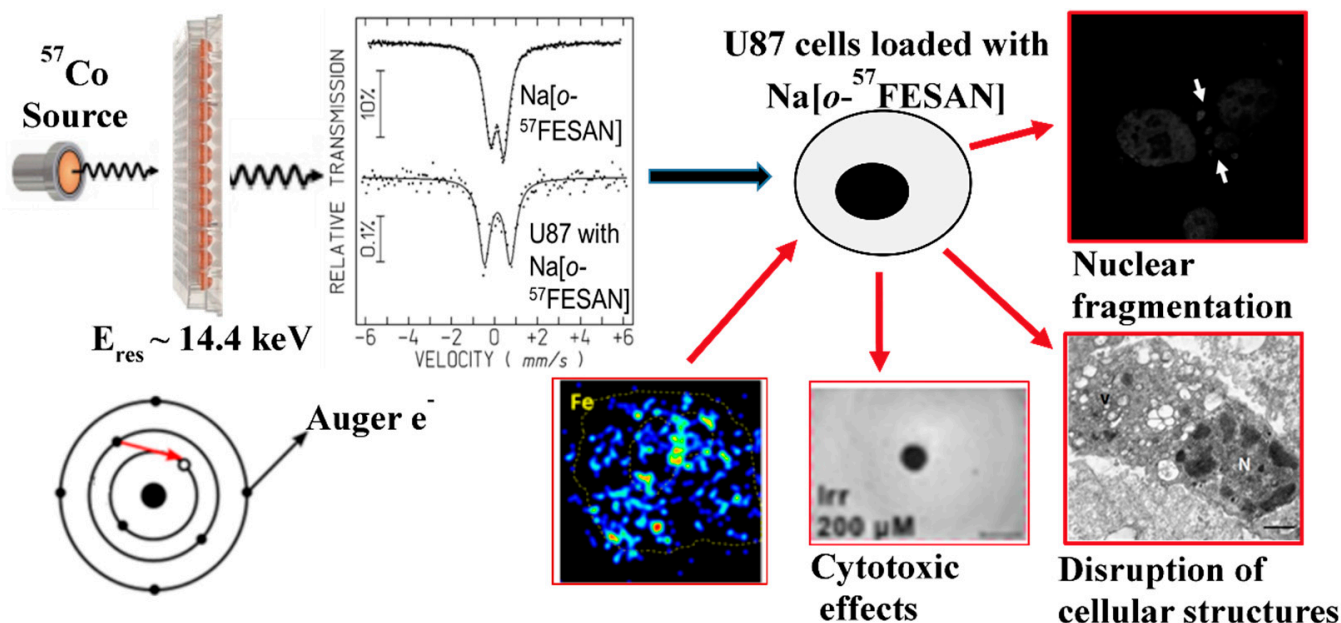
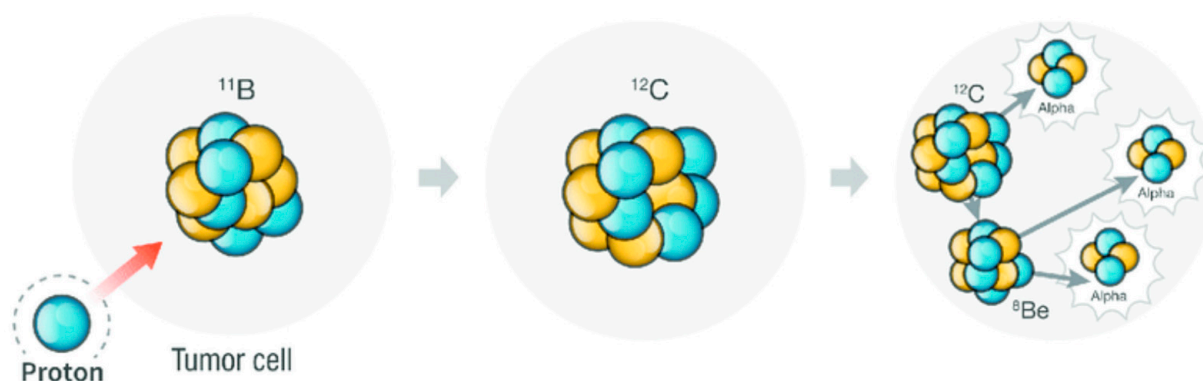


Figure 11. Mössbauer spectrum and 2D elemental maps of Fe distribution indicate that $[o\text{-}^{57}\text{FESAN}]^-$ is present inside U87 cells, an important requisite for selective energy deposition by Mössbauer absorption. Reproduced from [88] with permission from the Royal Society of Chemistry.

4.5. Proton Therapy Based on Boron

Proton therapy is an effective radiation treatment technique used in medicine, which consists of irradiating diseased tissue, most often to treat cancer, with a beam of protons [89,90]. Scheme 3 represents the Proton Boron Fusion Reaction (PBFR) between an energetic proton and ^{11}B resulting in the generation of three α particles. The viability of applying the proton boron fusion (PBF) reaction to the proton therapy to improve its effectiveness has been studied by using the Monte Carlo method [91–93] and experimentally using mercaptoundecahydro-closo-dodecaborate (abbreviated as BSH, which chemical formula is $[\text{SH-1-closo-B}_{12}\text{H}_{11}]^-$) [94]. Recently [95], taking advantage of the high ^{11}B isotope content in metallabis(dicarbollides), we tested, for the first time, metallacarboranes for the PBFR as a way to improve proton therapy with the $[o\text{-FESAN}]^-$ in the U87 glioblastoma cells. A simple calculation indicates that the use of PBFR would require 1/12 of isotopically natural molecules with respect to BNCT. Furthermore, in an ideal situation, BNCT can be used synchronously on the existing ^{10}B and Mössbauer on ^{57}Fe , resulting in multi therapies with only one compound. Results from the cellular damage response obtained suggest that PBFR radiation therapy, when applied to boron-rich compounds, is a promising modality to fight against resistant tumors.

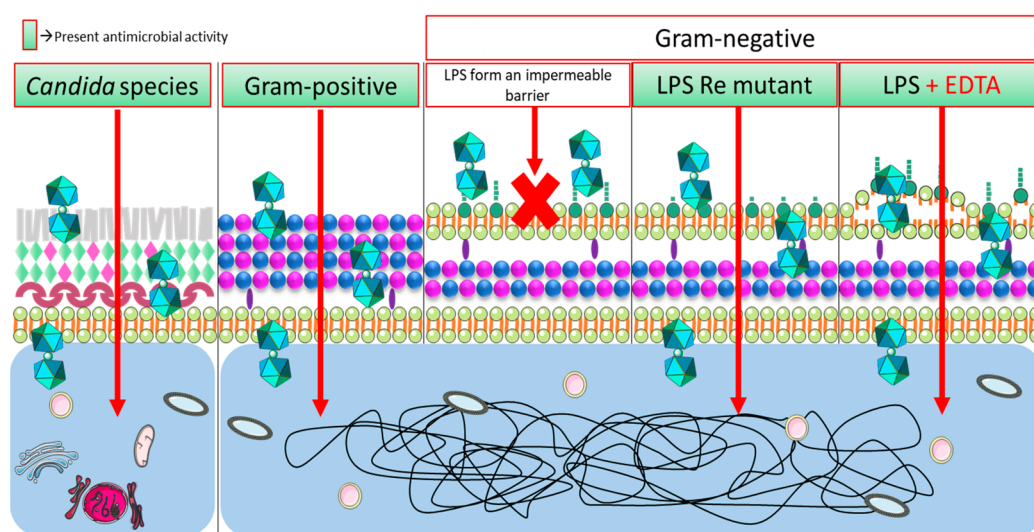


Scheme 3. Representation of the Proton Boron Fusion Reaction (PBFR). Blue circles represent protons while the yellow ones represent neutrons.

4.6. Antimicrobial Activity

In 2013, we started studying the physical–chemical properties and biological evaluation of the sodium salt of the small inorganic metallabis(dicarbollide) molecules ($[o\text{-COSAN}]^-$ and $[o\text{-FESAN}]^-$) and their derivatives $[8\text{-R}(\text{CH}_2\text{CH}_2\text{O})_2\text{-}o\text{-COSAN}]^-$ ($\text{R} = \text{-OOCCH}_3$; -OCH_3 ; $\text{-OCH}_2\text{CH}_3$) against pure cultures of 16 pathogenic bacterial strains (isolated from animals and humans as well as control strains) and 3 strains of *Candida* spp. as promising antimicrobial agents to tackle bacterial infections [96]. It is important to emphasize that the methicillin-resistant strain of *Staphylococcus aureus* (MRSA), the polyresistant strains of *Pseudomonas aeruginosa*, as well as of *Candida* spp., are sensitive to the compounds $\text{Na}[8\text{-CH}_3(\text{CH}_2\text{CH}_2\text{O})_2\text{-}o\text{-COSAN}]$ and $\text{Na}[8\text{-CH}_3\text{CH}_2(\text{CH}_2\text{CH}_2\text{O})_2\text{-}o\text{-COSAN}]$. Recently, a review of the increasing evidence that boron cluster compounds are promising antimicrobial (antibacterial and antifungal) agents appeared [97]. Lately, with the objective to establish a structure–activity relationship, which clearly supports the antimicrobial activity of the pristine metallabis(dicarbollide) complexes, we tested the small molecules $\text{Na}[o\text{-COSAN}]$, $\text{Na}[o\text{-FESAN}]$, $\text{Na}[m\text{-COSAN}]$, $\text{Na}[m\text{-FESAN}]$, the di-iodinated derivatives $\text{Na}[8,8'\text{-I}_2\text{-}o\text{-COSAN}]$, $\text{Na}[8,8'\text{-I}_2\text{-}o\text{-FESAN}]$ and polyanionic species incorporating one or two cobaltabis(dicarbollide) anions with activity against four *Gram-positive* bacteria (two *Enterococcus faecalis* strains and two of *Staphylococcus aureus* including Multi-Resistant *Staphylococcus Aureus* (MRSA) strains), five *Gram-negative* bacteria (three strains of *Escherichia coli* and two of *Pseudomonas aeruginosa*), and three *Candida albicans* strains that have been responsible for human infections [98,99]. We demonstrated an antimicrobial effect against *Candida* species (Minimum Inhibitory Concentration (MIC) of 2 and 3 nM for $\text{Na}[8,8'\text{-I}_2\text{-}o\text{-COSAN}]$ and $\text{Na}[m\text{-COSAN}]$, respectively), and against *Gram-positive* and *Gram-negative* bacteria, including multi-resistant MRSA strains (MIC of 6 nM for $\text{Na}[8,8'\text{-I}_2\text{-}o\text{-COSAN}]$). The selectivity index (abbreviated as SI and, calculated as the ratio $\text{IC}_{50}/\text{MIC}$) for antimicrobial activity of $\text{Na}[o\text{-COSAN}]$ and $\text{Na}[8,8'\text{-I}_2\text{-}o\text{-COSAN}]$ compounds is very high (165 and 1180, respectively), which reveals that these small anionic metallacarborane molecules may be useful to tackle antibiotic-resistant bacteria because it is considered that an $\text{SI} \geq 10$ is acceptable for a selective bioactive sample.

Furthermore, we demonstrated that the outer membrane of *Gram-negative* bacteria establishes an impermeable barrier for some of these metallabis(dicarbollide) small molecules (Scheme 4). Nonetheless, the addition of two iodine groups in the structure of the parent $\text{Na}[o\text{-COSAN}]$ had an improved effect (3–7 times) against *Gram-negative* bacteria. It is important to emphasize that the most active metallabis(dicarbollides) (*meta*-isomers $\text{Na}[m\text{-COSAN}]$, $\text{Na}[m\text{-FESAN}]$) and the di-iodinated derivatives $\text{Na}[8,8'\text{-I}_2\text{-}o\text{-COSAN}]$, $\text{Na}[8,8'\text{-I}_2\text{-}o\text{-FESAN}]$) are both *transoid* conformers in opposite to the $\text{Na}[o\text{-COSAN}]$ that is *cisoid* conformer (see Figure 1), which represent structures with particular physical–chemical properties that make these small molecules more permeable to this barrier.



Scheme 4. Graphical representation of the transport of small anionic metallabis(dicarbollide) molecules through microbiological membranes of *Candida* sp. (left), Gram-positive (center), and Gram-negative (right) [100].

The fact that these small molecules cross the mammalian membrane and have antimicrobial properties but low toxicity for mammalian cells (high selectivity index SI) represents a promising tool to treat infectious intracellular bacteria as there is an urgent need for new antibiotics discovery and development. This achievement represents a relevant advance in the field.

5. Boron Clusters-Based Dyes as Theranostic Agents for Diagnosis and Therapy

Today, one of the most important tools in predicting disease is diagnosis. Molecular imaging is a remarkable diagnostic tool in vitro and in vivo that could provide crucial biological information regarding a targeted disease and can thus help to establish a particular treatment or therapy [100,101]. Moreover, the development of theranostic systems to integrate imaging and therapy is an efficient strategy for real-time tracking of the pharmacokinetics and biodistribution of a drug. Current imaging modalities include optics (e.g., fluorescence, Raman, photoacoustics), X-ray, magnetic resonance, radionuclides, and mass spectrometry [102]. Among them, Fluorescence Bioimaging is a common modality for cell and tissue visualization, being of special interest in preclinical research on theranostic agents. In this context, each fluorophore has its benefits and drawbacks, which requires the continued search for new fluorescent probes to meet stringent necessities for applications in terms of sensitive and selective use for bioimaging applications.

Moreover, imaging-guided BNCT is a challenge as it allows us to know the accurate position of the boron-containing compound in the body as well as the accumulation in the tumor. Therefore, it is an important issue to label the boron-containing compound with a fluorescence tracer in order to have relevant information for both diagnosis and therapy [103–107]. In particular, the near-infrared (NIR) boron carriers are of great interest due to their deeper penetration into the living body and their ability to avoid interference from body tissues [108,109].

Dr. Núñez has been a staff member of the LMI group since 2001. Over this time, she has developed synthetic strategies for the functionalization of a great variety of scaffolds, i.e., star-shape molecules and dendrimers [28,110], octasilsesquioxanes [111–114], carbon-based materials [115,116], among others [117], with icosahedral boron clusters and studied their properties. In 2007, Dr. Núñez reported a set of blue emissive Fréchet-type aryl ether core molecules peripherally functionalized with *closo*-carborane and *nido*-carborane clusters [118,119]. It was then demonstrated that the maximum wavelength and emission intensity depend on the C_{cluster} substituent (Me or Ph), the solvent polarity, and the nature

of the cluster (*closo* or *nido*). This work was the beginning of her immersion in the field of luminescence. Since then, her main interest has been the development of photoluminescent boron cluster-based organic π -conjugated dyes [120–128], revealing that incorporation of neutral and anionic boron clusters into the structure of well-known fluorophores is an attractive chemical strategy to modulate and improve their photoluminescence properties [15,120–128]. Her current research interest is more focused on new boron-based molecules and materials as theranostic agents for diagnosis (bioimaging) and boron carriers for BNCT.

A set of BODIPY-anionic boron cluster conjugates bearing dianionic $[B_{12}H_{12}]^{2-}$ and monoanionic, $[o-COSAN]^{-}$ and $[o-FESAN]^{-}$ clusters were designed and synthesized to be used as fluorescent cell probes and BNCT anticancer agents (1–5 in Figure 12a) [129]. These conjugates were readily synthesized from the meso-(4-hydroxyphenyl)-4,4-difluoro-4-bora-3a,4a-diaza-s-indacene (BODIPY) by ring-opening reaction of the corresponding boron clusters derivatives. The luminescent properties of the BODIPY were not significantly altered by the linking of the anionic boron clusters, showing emission fluorescent quantum yields (Φ_F) in the range of 3–6%. Moreover, the cytotoxicity and cellular uptake of these compounds were analyzed *in vitro* at different concentrations of B (5, 50, and 100 $\mu\text{g B/mL}$) using HeLa cells. None of the compounds showed cytotoxicity at the lowest concentration (5 $\mu\text{g B/mL}$). Compound bearing $[B_{12}H_{12}]^{2-}$ and Na^+ as cation were non cytotoxic at any concentration, while the other compounds showed toxicity at the highest concentrations after 24h. Remarkably, all the compounds were successfully internalized by HeLa cells, exhibiting a strong cytoplasmic stain (Figure 12b). The internalization efficiency for all the compounds was assessed at the lowest concentration (5 $\mu\text{g B/mL}$), in which they are not cytotoxic. The exceptional cellular uptake and intracellular boron release, together with their fluorescent and biocompatibility properties, highlight the suitability of these boron cluster-containing dyes, especially $[o-COSAN]^{-}$ derivative, as potential candidates for cell labeling agents towards medical diagnosis in clinical biopsies. Moreover, the excellent cellular uptake, along with the boron-rich content of our conjugates, make them good candidates as boron carriers for BNCT.

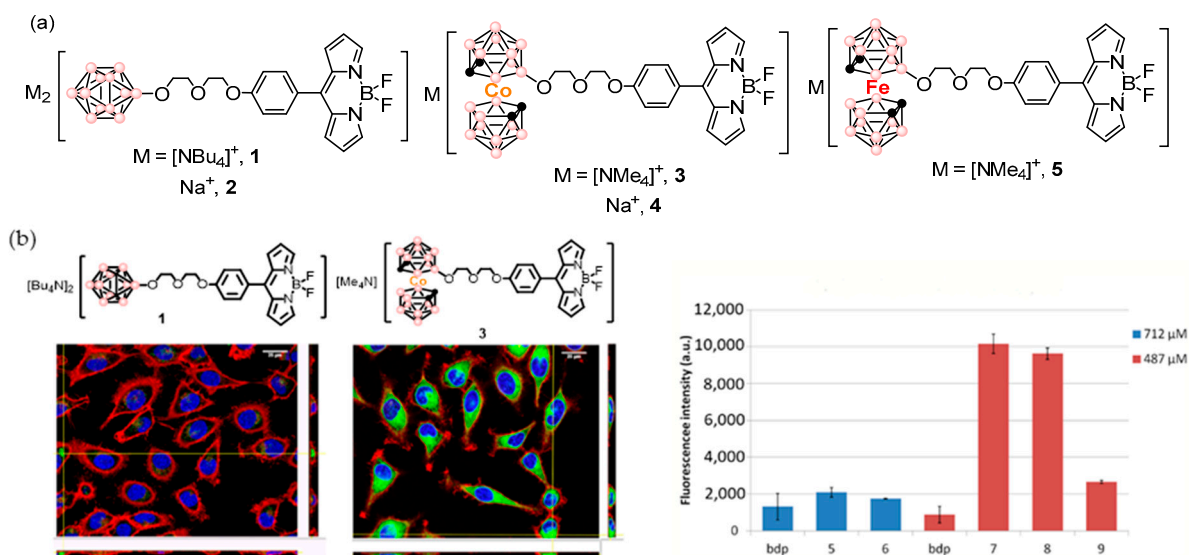


Figure 12. (a) Molecular structures of boron cluster-BODIPY conjugates 1–5 (pink circles in the cluster are B or B-H and black circles in the cluster are C-H). (b) Intracellular localization of BODIPY dyads 1 and 3 in HeLa cells obtained by confocal laser scanning microscopy (left). Cellular uptake comparison between BODIPY dye and BODIPY-boron clusters at 100 $\mu\text{g/mL}$ of B for each compound (CLSM) (left). Mean values and SD from three independent experiments. a.u.: arbitrary units (right). Reprinted (adapted) with permission from Ref. [129] *Bioconjugate Chem.* 2018, 29, 1763–1773. Copyright 2018, American Chemical Society.

Our interest in the development of new boron delivery systems to be used for biological applications led us to prepare a family of fluorescent organotin compounds that have shown excellent properties as nucleoli and cytoplasmic markers *in vitro* [130]. These organotin compounds are based on 4-hydroxy-*N'*-((2-hydroxynaphthalen-1-yl)methylene)benzohydrazidato that was derivatized to contain two different boron clusters, $[B_{12}H_{12}]^{2-}$ and $[o-COSAN]^{-}$ following the oxonium ring opening reaction (6–9 in Figure 13a). These compounds showed photoluminescence properties in solution with Φ_F values in the range from 24% to 49%. Remarkably, linking these anionic boron clusters to tin complexes improved their solubility in cell media, which resulted in better cell internalization and higher cellular uptake, as they do not aggregate either on the cell surface or in the extracellular media. Mouse melanoma B16F10 cells were incubated with 10 $\mu\text{g}/\text{mL}$ of the different compounds for 2 h and then analyzed by confocal laser microscopy. Noticeably different staining effect was observed depending on the type of boron cluster attached to the organotin complexes. Compound 8 bearing the $[o-COSAN]^{-}$ anion and two phenyl rings coordinated to the Sn showed an important fluorescence in the cytoplasm, whereas that bearing $[B_{12}H_{12}]^{2-}$ (6) produced extraordinary nucleoli and cytoplasmic staining (Figure 13b). The remarkable fluorescence staining properties of these organotin compounds in B16F10 cells make them excellent candidates for *in vitro* fluorescent bioimaging.

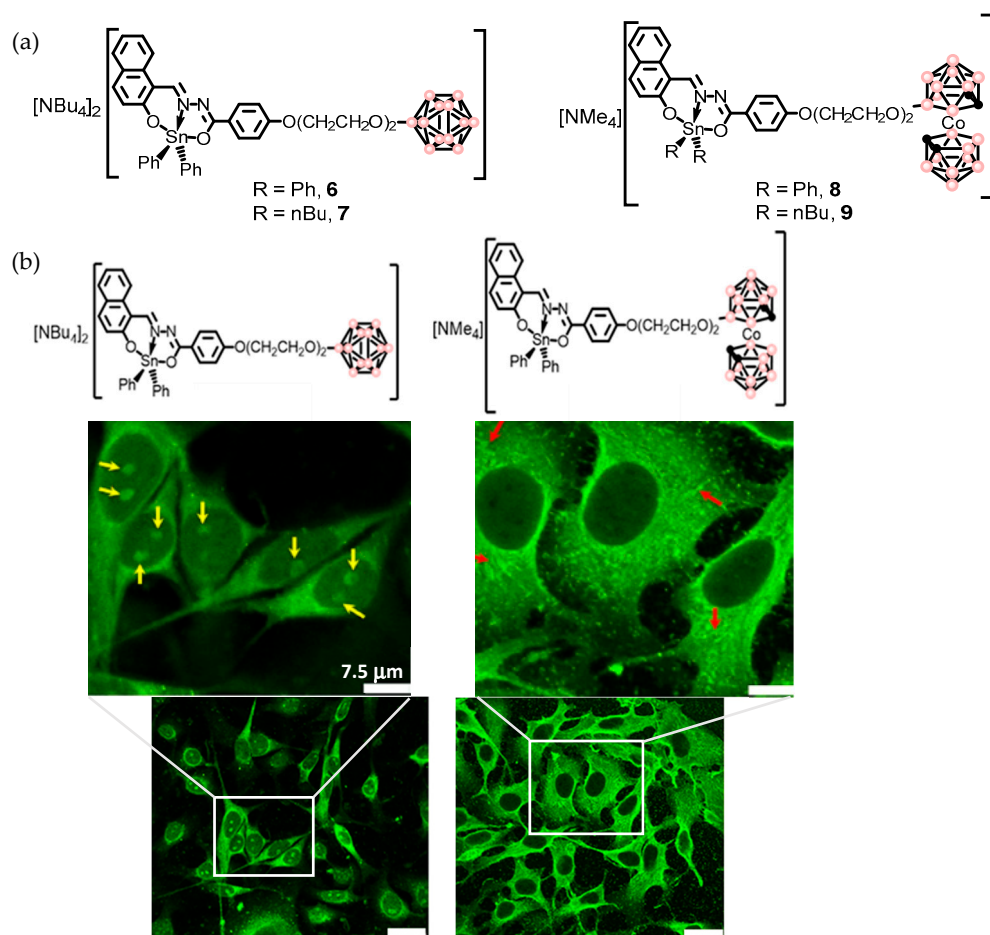


Figure 13. (a) Molecular structures of Tin complexes containing anionic boron clusters 6–9 (pink circles in the cluster are B or B-H, black circles in the cluster are C-H). (b) Cellular uptake of organotin compounds 6 and 8 bearing anionic $[B_{12}H_{12}]^{2-}$ (left) and $[o-COSAN]^{-}$ (right) by confocal laser scanning microscopy (CLSM). The yellow and red arrows show the internalization of our compounds in the cytoplasm and nucleoli [130]. Reprinted/adapted with permission from Ref. [130] Copyright 2018, Wiley.

Apart from previous BODIPY derivatives bearing anionic boron clusters, our group has also developed a family of neutral BODIPY-carboranyl conjugates which have been synthesized following Sonogashira or Heck cross-coupling reactions in which properly functionalized *ortho*- and *meta*-carborane clusters have been linked to light-emitting BODIPY or aza-BODIPY cores [131–133]. Figure 14 illustrates three different BODIPY-carboranyl systems with Ph-*ortho*-carborane (**10–11**) and Ph-*meta*-carborane (**12**), as examples. Due to their fluorescence properties, these fluorophores were studied *in vitro* as fluorescent probes. HeLa cells were incubated for 30 min with this set of BODIPYs, which presented very different behavior regarding cellular uptake and subcellular distribution (Figure 14) [132]. The differences seem to originate from their diverse static dipole moments and partition coefficients, which depend on the type of cluster isomer (*o*- or *m*-) linked to the BODIPY and that modulates the ability of these molecules to interact with the lipophilic microenvironments in cells. It can be highlighted that the *m*-carborane derivative with higher lipophilicity was much better internalized by cells than their *ortho* analogs. Confocal images of HeLa cells incubated with **12** (Figure 14) clearly indicate that **12** is accumulated in the cytoplasm of the cell. This evidence provides a molecular design strategy for improving the prospective applications of BODIPY-carboranyl dyads as potential fluorescence *in vitro* bioimaging agents and boron carriers for BNCT, suggesting that *m*-isomers are potentially better theranostic agents than *o*-isomers.

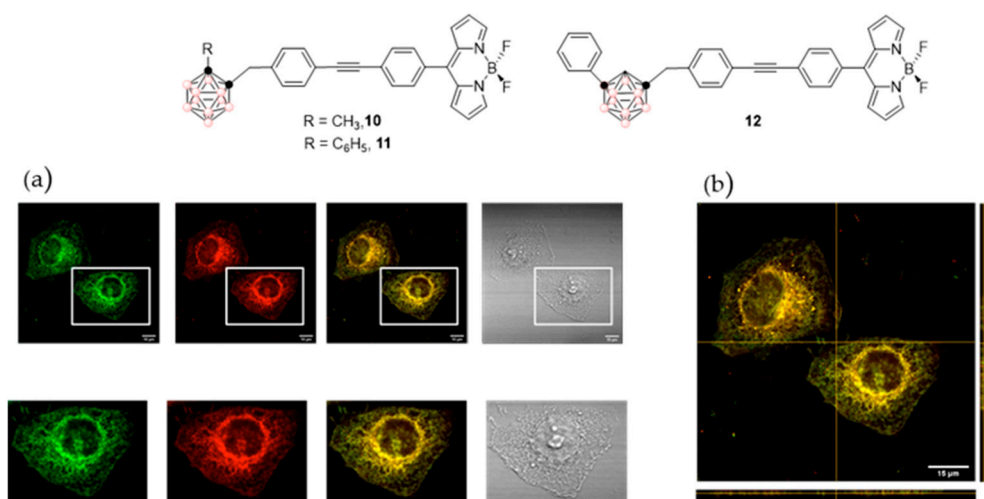


Figure 14. Molecular structures of the representative compounds: **10**, **11**, and **12** (top) ((pink circles in the cluster are B-H and black circles in the cluster are C)). Confocal images of 10 μM **12** in live HeLa cells after 30 min incubation: (a) Panels from left to right show the confocal green channel ($\lambda_{\text{exc}} = 486 \text{ nm}$, $\lambda_{\text{em}} = 500 \text{ nm}$), red channel ($\lambda_{\text{exc}} = 535 \text{ nm}$, $\lambda_{\text{em}} = 610 \text{ nm}$), merged and bright channels, respectively. Scale bars represent 10 and 15 μm . (b) z-stack visualization [132]. Reprinted/adapted with permission from Ref. [132] Copyright 2020, Wiley.

Another type of well-known fluorophores are anthracene derivatives that exhibit excellent luminescence properties that make them perfect scaffolds for optical applications. Our group has developed efficient blue light-emitting materials by combining the properties of anthracene and *m*-carborane [134]. Three different *m*-carborane-anthracene dyads, in which the carborane is non-iodinated, mono-iodinated, or di-iodinated at B atoms, and the anthracene fragment is linked to one $\text{C}_{\text{cluster}}$ atom through a CH_2 spacer, were prepared. All of them exhibited exceptional fluorescence properties with high quantum yields ($\Phi_{\text{F}} \sim 100\%$) in solution with maximum emission of around 415 nm, confirming that simply linking the *m*-carborane fragment to one fluorophore produces a significant enhancement of the fluorescence emission in the target compound. Notably, the three conjugates exhibited good fluorescence efficiencies in aggregate state with Φ_{F} in the range 19–23%, indicating that our dyads are extremely good emitters in solution, while maintaining the emission properties

in the aggregate state. Moreover, their cytotoxicity and cellular uptake in HeLa cells were evaluated. None of the compounds showed cytotoxicity at different concentrations for HeLa cells. Confocal microscopy studies confirmed that, although all compounds were internalized by cells via endocytosis, exhibiting high fluorescence emission intensity, the one with two iodo atoms is the one with a higher cellular uptake. This suggested that the presence of iodo units leads to a more efficient transport across the plasma membrane and a better internalization of the compounds. Figure 15 shows the autofluorescence of HeLa cells and fluorescence emitted by HeLa cells incubated with the diiodinated antracene-*m*-carborane. We then conclude that the di-iodinated compound is an excellent candidate as a fluorescent dye for bioimaging studies in fixed cells, and due to the high boron content and exceptional cellular uptake, it could be used as a potential anticancer agent for BNCT.

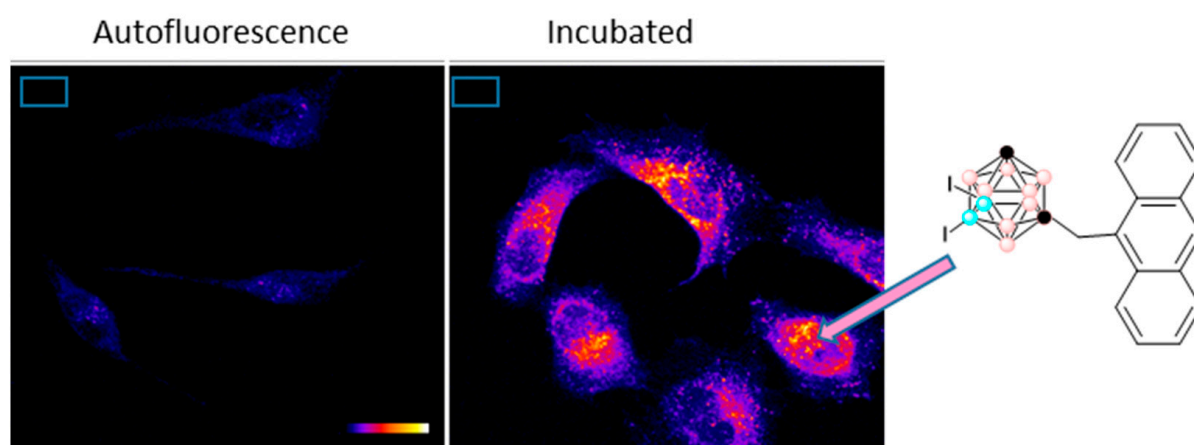
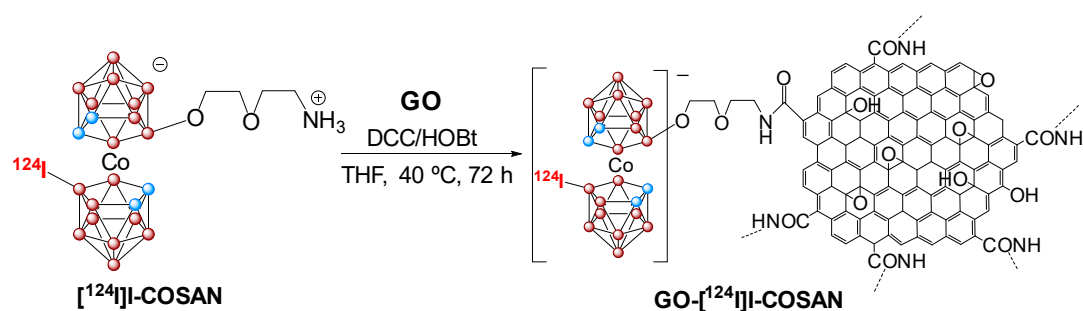


Figure 15. Fluorescence intensity emitted by HeLa cells incubated 4 h with 10 μM of diiodinated antracene-*m*-carborane. Image obtained with the confocal laser scanning microscope [134] (pink circles in the cluster are B-H, black circles in the cluster are C or C-H and blue circles in the cluster are B).

Besides previous luminescent materials, our group has also prepared carbon-based nanomaterials, which consist of graphene oxide (GO) functionalized on the surface by monoiodinated cobaltabis(dicarbollide) (GO-I-COSAN) for in vivo bioimaging. This GO-I-COSAN has been synthesized using the cobaltabis(dicarbollide) containing a B-I group and an amino group (I-COSAN) that is subsequently labeled with radioactive ^{124}I (Scheme 5) for its use in positron emission tomography (PET) [135]. After incubation of HeLa cells with different concentrations of GO-I-COSAN for 48 h, the results indicated that the nanomaterial was not cytotoxic, with cell mortality lower than 10%. Remarkably, internalization of the nanomaterial by cells was clearly confirmed by transmission electron microscopy (TEM), which showed that the GO-I-COSAN was accumulated in the cytoplasm without causing changes in either the size or morphology of the cells. Further in vivo studies using *C. elegans* indicated that GO-I-COSAN was ingested by the worms, showing no significant damage and very low toxicity, which supports the results observed in vitro. Radioisotopic labeling of I-COSAN using a palladium-catalyzed isotopic exchange reaction with $\text{Na}[^{124}\text{I}]\text{I}$ and its subsequent functionalization onto GO was performed successfully, leading to the formation of the radioactive nanocomposite GO- ^{124}I -I-COSAN (Scheme 5). The radiolabeled nanomaterial was injected into the mice, and PET images at different times were taken (Figure 16), which revealed no activity in the thyroid and stomach even at long times, indicating that iodide did not detach from the material. GO- ^{124}I -I-COSAN presented a favorable biodistribution profile, with long residence time on blood, mainly accumulated in the liver and slightly in the lung, and progressive elimination via the gastrointestinal tract. It is noteworthy that the high boron content of this material paves the way toward theranostics because it benefits traceable boron delivery for BNCT.



Scheme 5. Synthesis of the graphene oxide covalently bonded to the radiolabeled COSAN (pink circles in the cluster are B or B-H and blue circles in the cluster are C-H). Reprinted/adapted with permission from Ref. [135] Copyright 2021, American Chemical Society.

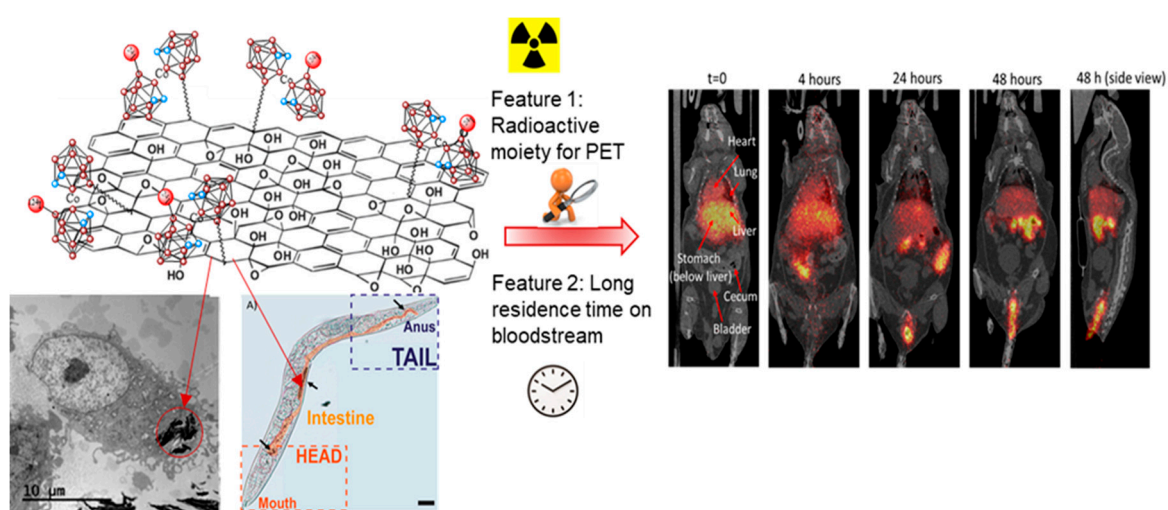


Figure 16. TEM image of GO-[^{124}I]I-COSAN internalized by HeLA cells, *C. elegans* incubated with GO-[^{124}I]I-COSAN and PET images of GO-[^{124}I]I-COSAN in the mice at different times (pink circles in the cluster are B or B-H, blue circles in the cluster are C-H and red circles exocenter at the ^{124}I). Reprinted/adapted with permission from Ref. [135] Copyright 2021, American Chemical Society.

Our group, in collaboration with S. Draper's group in Dublin, has also reported the preparation of transition metal-carborane photosensitizers by Sonogashira cross-coupling of (4-ethynylbenzyl)methyl-*o*-carborane with halogenated Ru(II)- or Ir(III)-phenanthroline complexes [136]. The resulting carboranyl-containing complexes (RuCB, IrCB, RuCB2, and IrCB2 in Figure 17) exhibited phosphorescence emission with maxima between 630 and 665 nm and lifetimes of 2.53, 0.38, 1.83, and 0.19 μs , respectively. All of them produce singlet oxygen with quantum yields (Φ_{Δ}) of 52%, 25%, 20%, and 10%, respectively, which suggests their use as triplet photosensitizers for photodynamic therapy (PDT). The subcellular uptake of all complexes was explored in SKBR-3 cells. Their localization and intensities were different depending on the number of carborane moieties and the nature of the transition metal centers. Complex IrCB was the best internalized with a clear accumulation in the cytoplasm. On the other hand, RuCB was hard to observe in the confocal microscopy images, but further microscopy experiments performed at a higher laser power showed that, in fact, RuCB was internalized. RuCB2 formed aggregates mainly located at the plasma membrane, whereas IrCB2 was poorly detected inside the cell (Figure 18). All of them showed the absence of dark toxicity under photodynamic therapy (PDT) conditions. Despite significant differences in the photophysical activities and cellular internalization of RuCB and IrCB, irradiation (λ_{ex} 405 nm; 3 min; mean intensity 55 μW) of both killed $\sim 50\%$ of SKBR-3 cells at 10 μM .

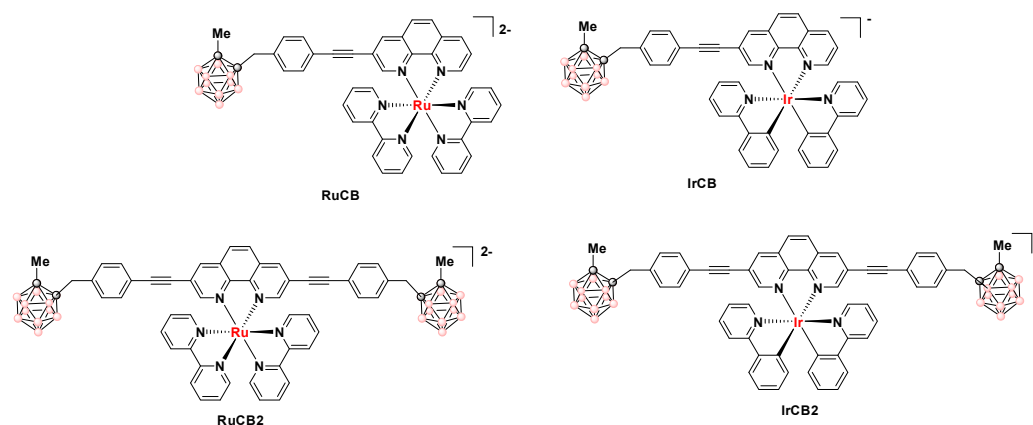


Figure 17. Structures of RuCB, IrCB, RuCB2, and IrCB2 (pink circles in the cluster are B-H and black circles in the cluster are C).

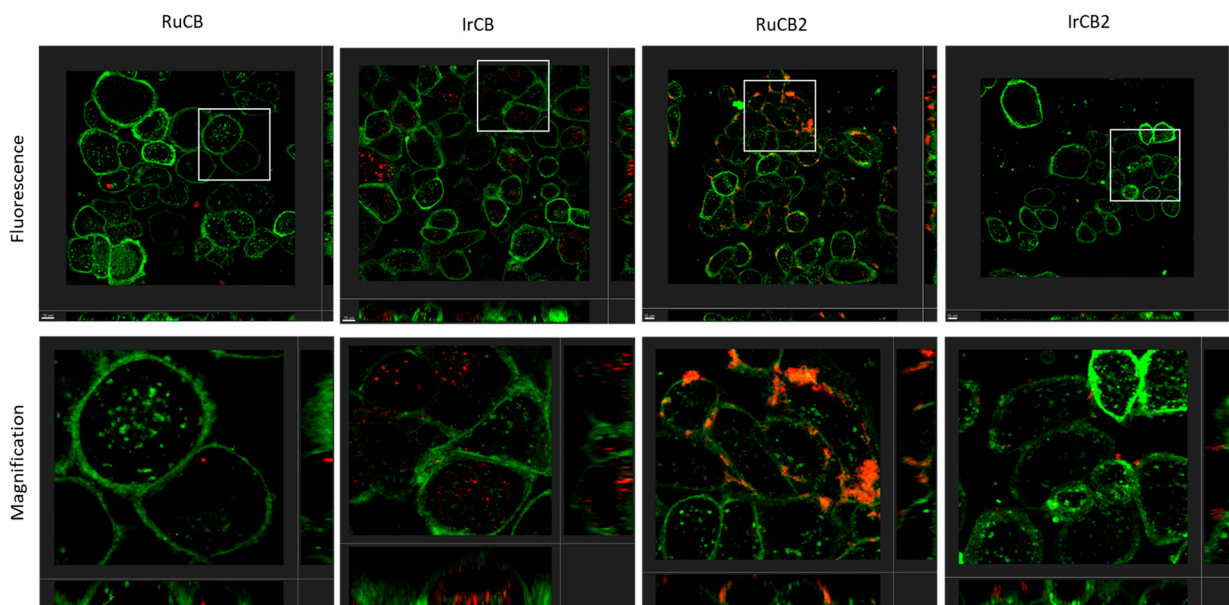


Figure 18. Orthogonal projection of z-stacks of live SKBR-3 cells incubated with 10 μM RuCB, IrCB, RuCB2, or IrCB2 for 4 h and observed under CLSM. (**Top row**): To analyze the localization of the compounds, fluorescence mode was used. Compound luminescence emission was detected in the range of 614–760 nm (red) by exciting the cells using the λ_{ex} 405 nm laser. Wheat Germ Agglutinin (WGA) fluorescence emission (membrane) was detected in the range of 496–579 nm (green) by exciting the cells using the λ_{ex} 488 nm laser. (**Bottom row**): Magnification of the selected areas (square boxes). Scale bar, 5 μm [136].

6. Conclusions

The progress in the synthesis of icosahedral boron clusters and their derivatives, the improvements in particles technology, the advances in medical imaging and computing, and the fact that new irradiation facilities are becoming available at hospitals makes radiotherapies such as BNCT and PBFV viable choices for new cancer medical therapies especially indicated for tumors resistant to chemotherapy and conventional radiotherapy. All this evidence promises to make BNCT and PBFV cutting-edge technology readily more accessible in the near future.

The fact that the icosahedral metallabis(dicarbollide) clusters reported in this review cross the mammalian membrane and have antimicrobial properties but low toxicity for mammalian cells (high selectivity index, SI) represents a promising tool to treat infectious intracellular bacteria. As there is an urgent need for antibiotic discovery and development,

these small anionic molecules represent relevant and promising antimicrobial agents to tackle bacterial infections.

This review also gathers several families of boron clusters-based fluorophores with luminescent properties as potential theranostic agents for bioimaging and BNCT. Among them are a series of BODIPYs functionalized with either neutral or anionic boron clusters, a set of anthracene-*m*-carborane dyads, and a family of tin complexes linked to anionic boron clusters. All of them showed excellent fluorescence emission and high cellular uptake. The preparation and study of GO functionalized with radiolabeled cobaltabis(dicarbollide) for PET are described. To end, a set of Ru(II) and Ir(III)-phenanthroline photosensitizers bearing one or two Me-*o*-carborane cages, as well as the in vitro studies for PDT are reported.

Author Contributions: C.V. and F.T. developed the idea. C.V. and R.N. wrote the draft. C.V., F.T. and R.N. assembled the article and gave it in its final form. All authors have read and agreed to the published version of the manuscript.

Funding: This work research was funded by the European Union's Horizon 2020 grant number 768686, the Spanish Ministerio de Economía y Competitividad grant number PID2019-106832RB-I00 and, the Generalitat de Catalunya grant number 2017SGR1720.

Institutional Review Board Statement: Not applicable.

Informed Consent Statement: Not applicable.

Data Availability Statement: Not applicable.

Acknowledgments: This mini review is dedicated to Emeritus at University of Leeds John D. Kennedy on his 80th anniversary for his great contribution to the field of boron' clusters. F.T. and C.V. fondly remember the long and interesting evenings of discussion about B.-H.M. agostic bonds that we had in the early 1990s.

Conflicts of Interest: The authors declare no conflict of interest.

References

1. Davy, H. An account of some new analytical researches on the nature of certain bodies, particularly the alkalis, phosphorus, sulphur, carbonaceous matter, and the acids hitherto undecomposed: With some general observations on chemical theory. *Philos. Trans. Royal Soc.* **1809**, *99*, 39–104.
2. Berzelius, J. Undersökning af flusspatssyran och dess märkvärdigaste föreningar. *Proc. R. Soc.* **1824**, *12*, 46–98.
3. Garrett, D.E. *Borates: Handbook of Deposits, Processing, Properties, and Use*; Academic Press: San Diego, CA, USA, 1998.
4. Hobbs, D.Z.; Campbell, T.T.; Block, F.E. *Methods Used in Preparing Boron*; Bureau of Mines, US Department of the Interior: Pittsburgh, PA, USA, 1964.
5. World Boron Reserves as of 2022, by Major Countries. Available online: <https://www.statista.com/statistics/264982/world-boron-reserves-by-major-countries/> (accessed on 26 April 2023).
6. Major Countries in Boron Production from 2010 to 2022. Available online: <https://www.statista.com/statistics/264981/major-countries-in-boron-production/#statisticContainer> (accessed on 26 April 2023).
7. Viñas, C. The Uniqueness of Boron as a novel challenging element for drugs in pharmacology, medicine and for smart biomaterials. *Future Med. Chem.* **2013**, *5*, 617–619. [CrossRef]
8. Poater, J.; Sola, M.; Viñas, C.; Teixidor, F. Hückel's Rule of Aromaticity Categorizes Aromatic closo Boron Hydride Clusters. *Chem. Eur. J.* **2016**, *22*, 7437–7443. [CrossRef]
9. Poater, J.; Solà, M.; Viñas, C.; Teixidor, F. Aromaticity and Three-Dimensional Aromaticity: Two sides of the Same Coin? *Angew. Chem. Int. Ed.* **2014**, *53*, 12191–12195. [CrossRef]
10. Poater, J.; Viñas, C.; Bennour, I.; Escayola-Gordils, S.; Solà, M.; Teixidor, F. Too Persistent to Give Up: Aromaticity in Boron Clusters Survives Radical Structural Changes. *J. Am. Chem. Soc.* **2020**, *142*, 9396–9407. [CrossRef]
11. The Nobel Prize in Chemistry 1976. Available online: www.nobelprize.org/prizes/chemistry/1976/summary/ (accessed on 26 April 2023).
12. Mukherjee, S.; Thilagar, P. Stimuli and shape responsive 'boron-containing' luminescent organic materials. *J. Mat. Chem. C* **2016**, *4*, 2647–2662. [CrossRef]
13. Lu, S.I.; Hamerton, I. Recent developments in the chemistry of halogen-free flame retardant polymers. *Prog. Polym. Sci.* **2002**, *27*, 1661–1712. [CrossRef]
14. Nuñez, R.; Romero, I.; Teixidor, F.; Viñas, C. Icosahedral boron clusters: A perfect tool for the enhancement of polymer features. *Chem. Soc. Rev.* **2016**, *45*, 5147–5173. [CrossRef] [PubMed]

15. Nuñez, R.; Tarrés, M.; Ferrer-Ugalde, A.; de Biani, F.F.; Teixidor, F. Electrochemistry and Photoluminescence of Icosahedral Carboranes, Boranes, Metallacarboranes, and Their Derivatives. *Chem. Rev.* **2016**, *116*, 14307–14378. [CrossRef] [PubMed]
16. Chujo, Y.; Tanaka, K. New Polymeric Materials Based on Element-Blocks. *Bull. Chem. Soc. Jpn.* **2015**, *88*, 633–643. [CrossRef]
17. Brand, R.; Lunkenheimer, P.; Loidl, A. Relaxation dynamics in plastic crystals. *J. Chem. Phys.* **2002**, *116*, 10386–10401. [CrossRef]
18. Plešek, J. Potential applications of the boron cluster compounds. *Chem. Rev.* **1992**, *92*, 269–278. [CrossRef]
19. Barth, R.F.; Soloway, A.H.; Fairchild, R.G.; Brugger, R.M. Boron Neutron-Capture Therapy for Cancer—Realities and Prospects. *Cancer* **1992**, *70*, 2995–3007. [CrossRef] [PubMed]
20. Hawthorne, M.F. The role of chemistry in the development of boron neutron-capture therapy of cancer. *Angew. Chem. Int. Ed.* **1993**, *32*, 950–984. [CrossRef]
21. Hawthorne, M.F.; Maderna, A. Applications of radiolabeled boron clusters to the diagnosis and treatment of cancer. *Chem. Rev.* **1999**, *99*, 3421–3434. [CrossRef]
22. Valliant, J.F.; Guenther, K.J.; King, A.S.; Morel, P.; Schaffer, P.; Sogbein, O.O.; Stephenson, K.A. The medicinal chemistry of carboranes. *Coord. Chem. Soc.* **2002**, *232*, 173–230. [CrossRef]
23. Sivaev, I.; Bregadze, V.V. Polyhedral Boranes for Medical Applications: Current Status and Perspectives. *Eur. J. Inorg. Chem.* **2009**, *11*, 1433–1450. [CrossRef]
24. Leśnikowski, Z.J. Challenges and Opportunities for the Application of Boron Clusters in Drug Design. *J. Med. Chem.* **2016**, *59*, 7738–7758. [CrossRef]
25. Cerecetto, H.; Couto, M. Contemporary Diagnostic and Therapeutic Approaches. In *Glioma*; Omerhodzic, I., Arnautovic, K., Eds.; IntechOpen Ltd.: London, UK, 2019.
26. Hosmane, N.S. *Boron Science, New Technologies and Applications*, 1st ed.; CRC Press Taylor&Francis Group: Boca Raton, FL, USA, 2012. [CrossRef]
27. Axtell, J.C.; Saleh, L.M.A.; Qian, E.A.; Wixtrom, A.I.; Spokoynny, A.M. Synthesis and Applications of Perfunctionalized Boron Clusters. *Inorg. Chem.* **2018**, *57*, 2333–2350. [CrossRef]
28. Viñas, C.; Nuñez, R.; Bennour, I.; Teixidor, F. Periphery Decorated and Core Initiated Neutral and Polyanionic Borane Large Molecules: Forthcoming and Promising Properties for Medicinal Applications. *Curr. Med. Chem.* **2019**, *26*, 5036–5076. [CrossRef]
29. Gozzi, M.; Schwarze, B.; Hey-Hawkins, E. Preparing (Metalla)carboranes for Nanomedicine. *ChemMedChem* **2021**, *16*, 1533–1565. [CrossRef] [PubMed]
30. Wolfgang, A.; Sauerwein, G.; Sancey, L.; Hey-Hawkins, E.; Kellert, M.; Panza, L.; Imperio, D.; Balcerzyk, M.; Rizzo, G.; Scalco, E.; et al. Theranostics in Boron Neutron Capture Therapy. *Life* **2021**, *11*, 330. [CrossRef]
31. Murphy, N.; McCarthy, E.; Dwyer, R.; Farràs, P. Boron clusters as breast cancer therapeutics. *J. Inorg. Biochem.* **2021**, *218*, 111412. [CrossRef]
32. Marfavi, A.; Kavianpour, P.; Rendina, L. Carboranes in drug discovery, chemical biology and molecular imaging. *Nat. Rev. Chem.* **2022**, *6*, 486–504. [CrossRef]
33. Hey-Hawkins, E.; Viñas, C. *Boron-Based Compounds: Potential and Emerging Applications in Medicine*; John Wiley & Sons, Ltd.: Oxford, UK, 2018.
34. ICMAB-CSIC. Available online: <https://lmi.icmab.es/> (accessed on 26 April 2023).
35. Grimes, R.N. *Carboranes*, 3rd ed.; Elsevier Inc.: New York, NY, USA, 2016.
36. Teixidor, F.; Viñas, C.; Démonceau, A.; Nuñez, R. Boron clusters: Do they receive the deserved interest? *Pure Appl. Chem.* **2003**, *75*, 1305–1313. [CrossRef]
37. Olid, D.; Nuñez, R.; Viñas, C.; Teixidor, F. Methods to produce B-C, B-P, B-N and B-S bonds in boron clusters. *Chem. Soc. Rev.* **2013**, *42*, 3318–3336. [CrossRef] [PubMed]
38. Sivaev, I.B.; Bregadze, V.I.; Sjöberg, S. Chemistry of closo-dodecaborate anion [B₁₂H₁₂](2-): A review. *Collect. Czechoslov. Chem. Commun.* **2002**, *67*, 679–727. [CrossRef]
39. Sivaev, I.B.; Bregadze, V.I. Chemistry of cobalt bis(dicarbollides). A review. *Collect. Czechoslov. Chem. Commun.* **1999**, *64*, 783–805. [CrossRef]
40. Sivaev, I.B.; Bregadze, V.I. Chemistry of nickel and iron bis(dicarbollides). A review. *Collect. Czechoslov. Chem. Commun.* **2002**, *614*, 27–36. [CrossRef]
41. Fisher, S.P.; Tomich, A.W.; Lovera, S.O.; Kleinsasser, J.F.; Guo, J.; Asay, M.J.; Nelson, H.M.; Lavallo, V. Nonclassical Applications of closo-Carborane Anions: From Main Group Chemistry and Catalysis to Energy Storage. *Chem. Rev.* **2019**, *119*, 8262–8290. [CrossRef] [PubMed]
42. Fisher, S.P.; Tomich, A.W.; Guo, J.; Lavallo, V. Teaching an old dog new tricks: New directions in fundamental and applied closo-carborane anion chemistry. *Chem. Commun.* **2019**, *55*, 1684–1701. [CrossRef]
43. Zhang, X.; Yan, H. Transition metal-induced B-H functionalization of o-carborane. *Coord. Chem. Rev.* **2019**, *378*, 466–482. [CrossRef]
44. Quan, Y.J.; Xie, Z.W. Controlled functionalization of o-carborane via transition metal catalyzed B-H activation. *Chem. Soc. Rev.* **2019**, *48*, 3660–3673. [CrossRef]
45. Qiu, Z.Z.; Xie, Z.W. A Strategy for Selective Catalytic B-H Functionalization of o-Carboranes. *Acc. Chem. Res.* **2021**, *54*, 4065–4079. [CrossRef]

46. Qiu, Z.Z.; Xie, Z.W. Functionalization of o-carboranes via carboryne intermediates. *Chem. Soc. Rev.* **2022**, *51*, 3164–3180. [[CrossRef](#)] [[PubMed](#)]
47. Dziejczak, R.M.; Spokoyny, A.M. Metal-catalyzed cross-coupling chemistry with polyhedral boranes. *Chem. Commun.* **2019**, *55*, 430–442. [[CrossRef](#)] [[PubMed](#)]
48. Endo, Y.; Iijima, T.; Yamakoshi, Y.; Yamaguchi, M.; Fukasawa, H.; Shudo, K. Potent Estrogenic Agonists Bearing Dicarba-closo-dodecaborane as a Hydrophobic Pharmacophore. *J. Med. Chem.* **1999**, *42*, 1501–1504. [[CrossRef](#)]
49. Endo, Y.; Iijima, T.; Yamakoshi, Y.; Kubo, A.; Itai, A. Structure-activity Study of Estrogenic Agonist Bearing Dicarba-closo-dodecaborane. Effect of Geometry and Separation Distance of Hydroxyl Groups at the Ends of Molecules. *Bioorg. Med. Chem. Lett.* **1999**, *9*, 3313–3318. [[CrossRef](#)]
50. Hawthorne, M.F. *Advances in Boron Chemistry*; Special Publication No. 201; Siebert, W., Ed.; Royal Society of Chemistry: London, UK, 1997; p. 261.
51. Endo, Y.; Yamamoto, K.; Kagechika, H. Utility of boron clusters for drug design. Relation between estrogen receptor binding affinity and hydrophobicity of phenols bearing various types of carboranyl groups. *Bioorg. Med. Chem. Lett.* **2003**, *13*, 4089–4092. [[CrossRef](#)]
52. Issa, F.; Kassiou, M.; Rendina, L.M. Boron in drug discovery: Carboranes as unique pharmacophores in biologically active compounds. *Chem. Rev.* **2011**, *111*, 5701–5722. [[CrossRef](#)] [[PubMed](#)]
53. Scholz, M.; Hey-Hawkins, E. Carboranes as pharmacophores: Properties, synthesis, application strategies. *Chem. Rev.* **2011**, *111*, 7035–7062. [[CrossRef](#)] [[PubMed](#)]
54. King, R.B. Three-dimensional aromaticity in polyhedral boranes and related molecules. *Chem. Rev.* **2001**, *101*, 1119–1152. [[CrossRef](#)] [[PubMed](#)]
55. Junqueira, G.M.A. Remarkable aromaticity of cobaltbis(dicarbollide) derivatives: A NICS study. *Theor. Chem. Acc.* **2018**, *137*, 92. [[CrossRef](#)]
56. Stoica, A.; Viñas, C.; Teixidor, F. Cobaltabisdicarbollide anion receptor for enantiomer-selective membrane electrode. *Chem Commun.* **2009**, *33*, 4988–4990. [[CrossRef](#)]
57. Stoica, A.; Viñas, C.; Teixidor, F. Application of the cobaltabisdicarbollide anion to the development of ion selective PVC membrane electrodes for tuberculosis drug analysis. *Chem. Commun.* **2008**, *48*, 6492–6494. [[CrossRef](#)]
58. Stoica, A.; Kleber, C.; Viñas, C.; Teixidor, F. Ion selective electrodes for protonable nitrogen containing analytes: Metallacarboranes as active membrane components. *Electrochim. Acta* **2013**, *113*, 94–98. [[CrossRef](#)]
59. Halima, H.B.; Baraket, A.; Viñas, C.; Zine, N.; Bausells, J.; Jaffrezic-Renault, N.; Teixidor, F.; Errachid, A. Selective Antibody-Free Sensing Membranes for Picogram Tetracycline Detection. *Biosensors* **2023**, *13*, 71. [[CrossRef](#)]
60. Garcia-Mendiola, T.; Bayon-Pizarro, V.; Zaulet, A.; Fuentes, I.; Pariente, F.; Teixidor, F.; Viñas, C.; Lorenzo, E. Metallacarboranes as tunable redox potential electrochemical indicators for screening of gene mutation. *Chem. Sci.* **2016**, *7*, 5786–5797. [[CrossRef](#)]
61. Pepiol, A.; Teixidor, F.; Saralidze, K.; van der Mare, C.; Willems, P.; Voss, L.; Knetsch, M.L.W.; Vinas, C.; Koole, L.H. A highly radiopaque vertebroplasty cement using tetraiodinated o-carborane additive. *Biomaterials* **2011**, *32*, 6389–6398. [[CrossRef](#)]
62. Farràs, P.; Cioran, A.M.; Sícha, V.; Teixidor, F.; Stibr, B.; Gruner, B.; Viñas, C. Metallacarboranes as Building Blocks for Polyanionic Polyarmed Aryl-Ether Materials. *Inorg. Chem.* **2008**, *47*, 9497–9508. [[CrossRef](#)]
63. Teixidor, F.; Sillanpää, R.; Pepiol, A.; Lupu, M.; Viñas, C. Synthesis of Globular Precursors. *Chem. Eur. J.* **2015**, *21*, 12778–12786. [[CrossRef](#)] [[PubMed](#)]
64. Teixidor, F.; Pepiol, A.; Viñas, C. Synthesis of periphery-decorated and core-initiated borane polyanionic macromolecules. *Chem. Eur. J.* **2015**, *21*, 10650–10653. [[CrossRef](#)]
65. Teixidor, F.; Viñas, C. *Handbook of Boron Science. With Applications in Organometallics, Catalysis, Materials and Medicine*; Halogenated Icosahedral Carboranes: A Platform for Remarkable Applications; Hosmane, N., Eagling, R., Eds.; World Scientific Publishing: London, UK, 2019; Volume 1.
66. Couto, M.; Alamón, C.; García, M.F.; Kovacs, M.; Trias, E.; Nievas, S.; Pozzi, E.; Curotto, P.; Thorp, S.; Dargosa, M.A.; et al. Closo-carboranyl-and Metallacarboranyl(1,2,3)-triazolyl-decorated Lapatinib-scaffold for Cancer Therapy Combining Tyrosine Kinase Inhibition and Boron Neutron Capture Therapy. *Cells* **2020**, *9*, 1408. [[CrossRef](#)] [[PubMed](#)]
67. Couto, M.; Alamón, C.; Nievas, S.; Perona, M.; Dargosa, M.A.; Teixidor, F.; Cabral, P.; Viñas, C.; Cerecetto, H. Bimodal Therapeutic Agent against Glioblastoma, one the most Lethal Cancer. *Chem. Eur. J.* **2020**, *26*, 14335–14340. [[CrossRef](#)]
68. Alamón, C.; Dávila, B.; García, M.F.; Sánchez, C.; Kovacs, M.; Trias, E.; Barbeito, L.; Gabay, M.; Zeineh, N.; Gavish, M.; et al. Sunitinib containing carborane pharmacophore with ability to inhibit tyrosine kinases receptors, FLT3, KIT, and PDGFR- β , exhibits powerful in vivo anti-glioblastoma activity. *Cancers* **2020**, *12*, 3423. [[CrossRef](#)]
69. Teixeira, R.G.; Marques, F.; Robaloc, M.P.; Fontrodona, X.; Garcia, M.H.; Geninatti Crich, S.; Viñas, C.; Valente, A. Ruthenium carboranyl complexes with 2,2'-bipyridine derivatives for potential bimodal therapy application. *RSC Adv.* **2020**, *10*, 16266–16276. [[CrossRef](#)] [[PubMed](#)]
70. Viñas, C.; Teixidor, F.; Nuñez, R. Boron clusters-based metallodendrimers. *Inorg. Chim. Acta* **2014**, *409*, 12–25. [[CrossRef](#)]
71. Cioran, A.M.; Musteti, A.D.; Teixidor, F.; Krpetić, Z.; Prior, I.A.; He, Q.; Kiely, C.J.; Brust, M.; Viñas, C. Mercaptocarborane-Capped Gold Nanoparticles: Electron Pools and Ion Traps with Switchable Hydrophilicity. *J. Am. Chem. Soc.* **2012**, *134*, 212–221. [[CrossRef](#)]
72. Oleshkevich, E.; Teixidor, F.; Rosell, A.; Viñas, C. Merging Icosahedral Boron Clusters and Magnetic Nanoparticles: Aiming toward Multifunctional Nanohybrid Materials. *Inorg. Chem.* **2018**, *57*, 462–470. [[CrossRef](#)]

73. Oleshkevich, E.; Moranco, A.; Galenkamp, K.M.O.; Grayston, A.; Gennatti Crich, S.; Alberti, D.; Protti, N.; Comella, J.X.; Teixidor, F.; Rosell, A.; et al. Combining magnetic nanoparticles and icosahedral boron clusters in biocompatible inorganic nanohybrids for cancer therapy. *Nanomedicine* **2019**, *20*, 101986. [[CrossRef](#)]
74. Grzelczak, M.P.; Danks, S.P.; Klipp, R.C.; Belic, D.; Zaulet, Z.; Kunstmann-Olsen, C.; Bradley, D.F.; Tsukuda, T.; Viñas, C.; Teixidor, F.; et al. Ion Transport across Biological Membranes by Carborane-Capped Gold Nanoparticles. *ACS Nano* **2017**, *11*, 12492–12499. [[CrossRef](#)]
75. Saha, A.; Oleshkevich, E.; Viñas, C.; Teixidor, F. Biomimetic Inspired Core–Canopy Quantum Dots: Ions Trapped in Voids Induce Kinetic Fluorescence Switching. *Adv. Mat.* **2017**, *29*, 1704238. [[CrossRef](#)]
76. Bauduin, P.; Prevost, S.; Farràs, P.; Teixidor, F.; Diat, O.; Zemb, T. A Theta-Shaped Amphiphilic Cobaltabisdicarbollide Anion: Transition From Monolayer Vesicles to Micelles. *Angew. Chem. Int. Ed.* **2011**, *50*, 5298–5300. [[CrossRef](#)]
77. Verdià, C.; Alcaraz, A.; Aguilera, V.M.; Cioran, A.M.; Tachikawa, S.; Nakamura, H.; Teixidor, F.; Viñas, C. Amphiphilic COSAN and I2-COSAN crossing synthetic lipid membranes: Planar bilayers and liposomes. *Chem Commun* **2014**, *50*, 6700–6703. [[CrossRef](#)] [[PubMed](#)]
78. Tarrés, M.; Canetta, E.; Viñas, C.; Teixidor, F.; Harwood, A.J. Imaging in living cells using vB–H Raman spectroscopy: Monitoring COSAN uptake. *Chem. Commun.* **2014**, *50*, 3370–3372. [[CrossRef](#)] [[PubMed](#)]
79. Tarrés, M.; Canetta, E.; Paul, E.; Forbes, J.; Azzouni, K.; Teixidor, F.; Viñas, C.; Harwood, A.J. Biological interaction of living cells with COSAN-based synthetic vesicles. *Sci. Rep.* **2015**, *5*, 7804. [[CrossRef](#)] [[PubMed](#)]
80. Pedrosa, L.; Martínez-Rovira, I.; Yousef, I.; Diao, D.; Teixidor, F.; Stanzani, E.; Martínez-Soler, F.; Tortosa, A.; Sierra, A.; Gonzalez, J.J.; et al. Synchrotron-Based Fourier-Transform Infrared Micro-Spectroscopy (SR-FTIRM) Fingerprint of the Small Anionic Molecule Cobaltabis(dicarbollide) Uptake in Glioma Stem Cells. *Int. J. Mol. Sci.* **2021**, *22*, 9937. [[CrossRef](#)]
81. Fuentes, I.; Pujols, J.; Viñas, C.; Ventura, S.; Teixidor, F. Dual Binding Mode of Metallacarborane Produces a Robust Shield on Proteins. *Chem. Eur. J.* **2019**, *25*, 12820–12829. [[CrossRef](#)] [[PubMed](#)]
82. Goszczynski, T.M.; Fink, K.; Kowalski, K.; Lesnikowski, Z.J.; Boratynski, J. Interactions of Boron Clusters and their Derivatives with Serum Albumin. *Sci. Rep.* **2017**, *7*, 9800. [[CrossRef](#)]
83. Fuentes, I.; García-Mendiola, T.; Sato, S.; Pita, M.; Nakamura, H.; Lorenzo, E.; Teixidor, F.; Marques, F.; Viñas, C. Metallacarboranes on the Road to Anticancer Therapies: Cellular Uptake, DNA Interaction, and Biological Evaluation of Cobaltabisdicarbollide [COSAN][−]. *Chem. Eur. J.* **2018**, *24*, 17239–17254. [[CrossRef](#)] [[PubMed](#)]
84. Merhi, T.; Jonchere, A.; Girard, L.; Diat, O.; Nuez, M.; Viñas, C.; Bauduin, P. Highlights on the Binding of Cobalt-Bis-(Dicarbollide) with Glucose Units. *Chem. Eur. J.* **2020**, *26*, 13935–13947. [[CrossRef](#)] [[PubMed](#)]
85. Gona, K.B.; Zaulet, A.; Gomez-Vallejo, V.; Teixidor, F.; Llop, J.; Viñas, C. COSAN as a molecular imaging platform: Synthesis and “in vivo” imaging. *Chem. Commun.* **2014**, *50*, 11415–11417. [[CrossRef](#)]
86. Nuez-Martinez, M.; Pinto, C.I.G.; Guerreiro, J.F.; Mendes, F.; Marques, F.; Muñoz-Juan, A.; Xavier, J.A.M.; Laromaine, A.; Bitonto, V.; Protti, N.; et al. Cobaltabis(dicarbollide) ([o-COSAN][−]) as Multifunctional Chemotherapeutics: A Prospective Application in Boron Neutron Capture Therapy (BNCT) for Glioblastoma. *Cancers* **2021**, *13*, 6367. [[CrossRef](#)] [[PubMed](#)]
87. Winberg, K.J.; Barbera, G.; Eriksson, L.; Teixidor, F.; Tolmachev, V.; Viñas, C.; Sjöberg, S. High yield [¹²⁵I] iodide-labeling of iodinated carboranes by palladiumcatalyzed isotopic exchange. *J. Organomet. Chem.* **2003**, *680*, 188–192. [[CrossRef](#)]
88. Buades, A.B.; Pereira, L.C.J.; Vieira, B.J.C.; Cerdeira, A.C.; Waerenborgh, J.C.; Pinheiro, T.; Matos, A.P.A.; Pinto, C.G.; Guerreiro, J.F.; Mendes, F.; et al. The Mossbauer effect using Fe-57-ferrabisdicarbollide ([o-(57)FESAN]^(−)): A glance into the potential of a low-dose approach for glioblastoma radiotherapy. *Inorg. Chem. Front.* **2022**, *9*, 1490–1503. [[CrossRef](#)]
89. Paganetti, H. *Proton Therapy Physics*, 2nd ed.; Book series in Medical Physics and Biomedical Engineering; CRC Press: Boca Raton, FL, USA, 2020.
90. Yoon, D.-K.; Jung, J.-Y.; Suh, T.S. Application of proton boron fusion reaction to radiation therapy: A Monte Carlo simulation study. *Appl. Phys. Lett.* **2014**, *105*, 223507. [[CrossRef](#)]
91. Yoon, D.-K.; Naganawa, N.; Kimura, M.; Choi, M.-G.; Kim, M.-S.; Kim, Y.-J.; Law, M.W.-M.; Djeng, S.-K.; Shin, H.-B.; Choe, B.-Y.; et al. Application of proton boron fusion to proton therapy: Experimental verification to detect the alpha particles. *Appl. Phys. Lett.* **2019**, *115*, 223701. [[CrossRef](#)]
92. Shin, H.-B.; Yoon, D.-K.; Jung, J.-Y.; Kim, M.-S.; Suh, T.S. Prompt gamma ray imaging for verification of proton boron fusion therapy: A Monte Carlo study. *Phys. Med.* **2016**, *32*, 1271. [[CrossRef](#)]
93. Jung, J.-Y.; Yoon, D.-K.; Barraclough, B.; Lee, H.C.; Suh, T.S.; Lu, B. Comparison between proton boron fusion therapy (PBFT) and boron neutron capture therapy (BNCT): A Monte Carlo study. *Oncotarget* **2017**, *8*, 39774. [[CrossRef](#)]
94. Cirrone, G.A.P.; Manti, L.; Margarone, D.; Petringa, G.; Giuffrida, L.; Minopoli, A.; Picciotto, A.; Russo, G.; Cammarata, F.; Pisciotto, P.; et al. First experimental proof of Proton Boron Capture Therapy (PBCT) to enhance proton therapy effectiveness. *Sci. Rep.* **2018**, *8*, 1141. [[CrossRef](#)] [[PubMed](#)]
95. Nuez-Martinez, M.; Queralt-Martín, M.; Muñoz-Juan, A.; Aguilera, V.M.; Laromaine, A.; Teixidor, F.; Viñas, C.; Pinto, C.G.; Pinheiro, T.; Guerreiro, J.F.; et al. Boron clusters (ferrabisdicarbollides) shaping the future as radiosensitizers for multimodal (chemo/radio/PBFR) therapy of glioblastoma. *J. Mater. Chem. B* **2022**, *10*, 9727–9934. [[CrossRef](#)] [[PubMed](#)]
96. Popova, T.; Zaulet, A.; Teixidor, F.; Alexandrova, R.; Viñas, C. Investigations on antimicrobial activity of cobaltabisdicarbollides. *J. Organomet. Chem.* **2013**, *747*, 229–234. [[CrossRef](#)]

97. Fin, K.; Uchman, M. Boron cluster compounds as new chemical leads for antimicrobial Therapy. *Coord. Chem. Rev.* **2021**, *431*, 213684.
98. Romero, I.; Martínez-Medina, M.; Camprubi-Font, C.; Bennour, I.; Moreno, D.; Martínez-Martínez, L.; Teixidor, F.; Fox, M.A.; Viñas, C. Metallacarborane Assemblies as Effective Antimicrobial Agents, Including a Highly Potent Anti-MRSA Agent. *Organometallics* **2020**, *39*, 4253–4264. [[CrossRef](#)]
99. Bennour, I.; Ramos, M.N.; Nuez-Martínez, M.; Xavier, J.A.M.; Buades, A.B.; Sillanpää, R.; Teixidor, F.; Choquesillo-Lazarte, D.; Romero, I.; Martínez-Medina, M.; et al. Water soluble organometallic small molecules as promising antibacterial agents: Synthesis, physical–chemical properties and biological evaluation to tackle bacterial infections. *Dalton Trans.* **2022**, *51*, 7188–7209. [[CrossRef](#)]
100. Smith, B.R.; Gambhir, S.S. Nanomaterials for in vivo imaging. *Chem. Rev.* **2017**, *117*, 901–986. [[CrossRef](#)]
101. Fan, W.P.; Yung, B.; Huang, P.; Chen, X.Y. Nanotechnology for multimodal synergistic cancer therapy. *Chem. Rev.* **2017**, *117*, 13566–13638. [[CrossRef](#)]
102. Kunjachan, S.; Ehling, J.; Storm, G.; Kiessling, F.; Lammers, T. Noninvasive imaging of nanomedicines and nanotheranostics: Principles, progress, and prospects. *Chem. Rev.* **2015**, *15*, 10907–10937. [[CrossRef](#)]
103. Genady, A.R.; Ioppolo, J.A.; Azaam, M.M.; El-Zaria, M.E. New functionalized mercaptoundecahydrododecaborate derivatives for potential application in boron neutron capture therapy: Synthesis, characterization and dynamic visualization in cells. *Eur. J. Med. Chem.* **2015**, *93*, 574–583. [[CrossRef](#)]
104. Gao, D.; Aly, S.M.; Karsenti, P.-L.; Brisard, G.; Harvey, P.D. Application of the boron center for the design of a covalently bonded closely spaced triad of porphyrinfullerene mediated by dipyrromethane. *Dalton Trans.* **2017**, *46*, 6278–6290. [[CrossRef](#)]
105. Nakase, I.; Katayama, M.; Hattori, Y.; Ishimura, M.; Inaura, S.; Fujiwara, D.; Takatani-Nakase, T.; Fujii, I.; Futakie, S.; Kirihata, M. Intracellular target delivery of cell-penetrating peptide-conjugated dodecaborate for boron neutron capture therapy (BNCT). *Chem. Commun.* **2019**, *55*, 13955. [[CrossRef](#)] [[PubMed](#)]
106. Zhao, F.; Hu, K.; Shao, C.; Jin, G. Original boron cluster covalent with poly-zwitterionic BODIPYs for boron neutron capture therapy agent. *Polym. Test.* **2021**, *100*, 107269. [[CrossRef](#)]
107. Ruan, Z.; Liu, L.; Fu, L.; Xing, T.; Yan, L. An amphiphilic block copolymer conjugated with carborane and a NIR fluorescent probe for potential imaging-guided BNCT therapy. *Polym. Chem.* **2016**, *7*, 4411. [[CrossRef](#)]
108. Kalot, G.; Godard, A.; Busser, B.; Pliquett, J.; Broekgaarden, M.; Motto-Ros, V.; Wegner, K.D.; Resch-Genger, U.; Koster, U.; Denat, F.; et al. Aza-BODIPY: A new vector for enhanced theranostic boron neutron capture therapy Applications. *Cells* **2020**, *9*, 1953. [[CrossRef](#)] [[PubMed](#)]
109. Cabrera-González, J.; Xochitiotzi-Flores, E.; Viñas, C.; Teixidor, F.; García-Ortega, H.; Farfán, N.; Santillan, R.; Parella, T.; Núñez, R. High-Boron-Content Porphyrin-Cored Aryl Ether Dendrimers: Controlled Synthesis, Characterization, and Photophysical Properties. *Inorg. Chem.* **2015**, *54*, 5021–5031. [[CrossRef](#)]
110. Ferrer-Ugalde, A.; Juárez-Pérez, E.J.; Teixidor, F.; Viñas, C.; Núñez, R. Synthesis, Characterization, and Thermal Behavior of Carboranyl-Styrene Decorated Octasilsesquioxanes: Influence of the Carborane Clusters on Photoluminescence. *Chem. Eur. J.* **2013**, *19*, 17021–17030. [[CrossRef](#)]
111. Cabrera-González, J.; Sánchez-Arderiu, V.; Viñas, C.; Parella, T.; Teixidor, F.; Núñez, R. Redox active metallacarborane-decorated octasilsesquioxanes. Electrochemical and thermal properties. *Inorg. Chem.* **2016**, *55*, 11630–11634. [[CrossRef](#)]
112. Cabrera-González, J.; Ferrer-Ugalde, A.; Bhattacharyya, S.; Chaari, M.; Teixidor, F.; Gierschner, J.; Núñez, R. Fluorescent carborane-vinylstilbene functionalised octasilsesquioxanes: Synthesis, structural, thermal and photophysical properties. *J. Mater. Chem. C* **2017**, *5*, 10211–10219. [[CrossRef](#)]
113. Cabrera-González, J.; Teixidor, F.; Viñas, C.; Núñez, R. Blue emitting star-shaped and octasilsesquioxane-based polyanions bearing boron clusters. Photophysical and thermal properties. *Molecules* **2020**, *25*, 1210. [[CrossRef](#)]
114. Cabana, L.; González-Campo, A.; Ke, X.; Van Tendeloo, G.; Núñez, R.; Tobias, G. Efficient Chemical Modification of Carbon Nanotubes with Metallacarboranes. *Chem. Eur. J.* **2015**, *21*, 16792–16795. [[CrossRef](#)]
115. Cabrera-González, J.; Cabana, L.; Ballesteros, B.; Tobias, G.; Núñez, R. Highly Dispersible and Stable Anionic Boron Cluster–Graphene Oxide Nanohybrids. *Chem. Eur. J.* **2016**, *22*, 5096–5101. [[CrossRef](#)] [[PubMed](#)]
116. Ferrer-Ugalde, A.; González-Campo, A.; Planas, J.G.; Viñas, C.; Teixidor, F.; Sáez, I.M.; Núñez, R. Tuning the Liquid Crystallinity of Cholesteryl-o-Carborane Dyads: Synthesis, Structure, Photoluminescence, and Mesomorphic Properties. *Crystals* **2021**, *11*, 133. [[CrossRef](#)]
117. Lerouge, F.; Viñas, C.; Teixidor, F.; Núñez, R.; Abreu, A.; Xochitiotzi, E.; Santillán, R.; Farfán, N. High Boron Content Carboranyl-Functionalized Aryl Ether Derivatives Displaying Photoluminescent Properties. *Dalton Trans.* **2007**, 1898–1903. [[CrossRef](#)] [[PubMed](#)]
118. Lerouge, F.; Ferrer-Ugalde, A.; Viñas, C.; Teixidor, F.; Núñez, R.; Abreu, A.; Xochitiotzi, E.; Santillán, R.; Farfán, N. Synthesis and Fluorescence Emission of Neutral and Anionic Di- and Tetra-Carboranyl Compounds. *Dalton Trans.* **2011**, *40*, 7541–7550. [[CrossRef](#)] [[PubMed](#)]
119. Ferrer-Ugalde, A.; Juárez-Pérez, E.J.; Teixidor, F.; Viñas, C.; Sillanpää, R.; Pérez-Inestrosa, E.; Núñez, R. Synthesis and Characterization of New Fluorescent Styrene-Containing Carborane Derivatives: The Singular Quenching Role of a Phenyl Substituent. *Chem. Eur. J.* **2012**, *18*, 544. [[CrossRef](#)]

120. Ferrer-Ugalde, A.; González-Campo, A.; Viñas, C.; Rodríguez-Romero, J.; Santillan, R.; Farfán, N.; Sillanpää, R.; Sousa-Pedrares, A.; Núñez, R.; Teixidor, F. Fluorescence of new o-carborane compounds with different fluorophores: Can it be tuned? *Chem. Eur. J.* **2014**, *20*, 9940–9951. [[CrossRef](#)]
121. Cabrera-González, J.; Viñas, C.; Haukka, M.; Bhattacharyya, S.; Gierschner, J.; Núñez, R. Photoluminescence in Carborane-Stilbene Triads: A Structural, Spectroscopic, and Computational Study. *Chem. Eur. J.* **2016**, *22*, 13588–13598. [[CrossRef](#)]
122. Ferrer-Ugalde, A.; Cabrera-González, J.; Juárez-Pérez, E.J.; Viñas, C.; Teixidor, F.; Pérez-Inestrosa, E.; Montenegro, J.M.; Sillanpää, R.; Haukka, M.; Núñez, R. Carborane-stilbene dyads: Influence of substituents and cluster isomers on the photoluminescent properties. *Dalton Trans.* **2017**, *46*, 2091–2104. [[CrossRef](#)]
123. Chaari, M.; Kelemen, Z.; Giner-Planas, J.; Teixidor, F.; Choquesillo-Lazarte, D.; Ben Salah, A.; Viñas, C.; Núñez, R. Photoluminescence in *m*-carborane–anthracene triads: A combined experimental and computational study. *J. Mater. Chem. C* **2018**, *6*, 11336–11347. [[CrossRef](#)]
124. Chaari, M.; Cabrera-González, J.; Kelemen, Z.; Ferrer-Ugalde, A.; Viñas, C.; Choquesillo-Lazarte, D.; Ben Salah, A.; Teixidor, F.; Núñez, R. Luminescence properties of carborane-containing distyrylaromatic systems. *J. Organomet. Chem.* **2018**, *865*, 206–213. [[CrossRef](#)]
125. Chaari, M.; Kelemen, Z.; Choquesillo-Lazarte, D.; Teixidor, F.; Viñas, C.; Núñez, R. Anthracene–styrene-substituted *m*-carborane derivatives: Insights into the electronic and structural effects of substituents on photoluminescence. *Inorg. Chem Front.* **2020**, *7*, 2370. [[CrossRef](#)]
126. Parejo, L.; Chaari, M.; Santiago, S.; Guirado, G.; Teixidor, F.; Núñez, R.; Hernando, J. Reversibly Switchable Fluorescent Molecular Systems Based on Metallacarborane–Perylene diimide Conjugates. *Chem. Eur. J.* **2021**, *27*, 270–280. Available online: <https://ddd.uab.cat/record/266062> (accessed on 26 April 2023). [[CrossRef](#)] [[PubMed](#)]
127. Soldevila-Sanmartín, J.; Ruiz, E.; Choquesillo-Lazarte, D.; Light, M.E.; Viñas, C.; Teixidor, F.; Núñez, R.; Pons, J.; Planas, J.G. Tuning the architectures and luminescence properties of Cu(I) compounds of phenyl and carboranyl pyrazoles: The impact of 2D versus 3D aromatic moieties in the ligand backbone. *J. Mater. Chem. C* **2021**, *9*, 7643–7657. [[CrossRef](#)]
128. Sinha, S.; Kelemen, Z.; Hümpfner, E.; Ratera, I.; Malval, J. –P.; Piers Jurado, J.; Viñas, C.; Teixidor, F.; Núñez, R. o-Carborane-based fluorophores as efficient luminescent systems both as solids and as water-dispersible nanoparticles. *Chem Comm.* **2022**, *58*, 4016–4019. [[CrossRef](#)]
129. Chaari, M.; Gaztelumendi, N.; Cabrera-González, J.; Peixoto-Moledo, P.; Viñas, C.; Xochitiotzi-Flores, E.; Farfan, N.; Ben Salah, A.; Nogués, C.; Núñez, R. Fluorescent BODIPY-anionic boron cluster conjugates as potential agents for cell tracking. *Bioconjugate Chem.* **2018**, *29*, 1763–1773. [[CrossRef](#)]
130. Cabrera-González, J.; Muñoz-Flores, B.M.; Viñas, C.; Chávez-Reyes, A.; Dias, H.V.R.; Jiménez-Pérez, V.M.; Núñez, R. Organotin dyes bearing anionic boron clusters as cell-staining fluorescent probes. *Chem. Eur. J.* **2018**, *4*, 5601–5612. [[CrossRef](#)]
131. Bellomo, C.; Chaari, M.; Cabrera-González, J.; Blangetti, M.; Lombardi, C.; Deagostino, A.; Viñas, C.; Gaztelumendi, N.; Nogués, C.; Núñez, R.; et al. Carborane-BODIPY dyads: New photoluminescent materials through an efficient Heck coupling. *Chem. Eur. J.* **2018**, *24*, 15622–15630. [[CrossRef](#)]
132. Labra-Vázquez, P.; Flores-Cruz, R.; Galindo-Hernández, A.; Cabrera-González, J.; Guzmán-Cedillo, C.; Jiménez-Sánchez, A.; Lacroix, P.G.; Santillan, R.; Farfán, N.; Núñez, R. Tuning the cell uptake and subcellular distribution in BODIPY–carboranyl dyads: An experimental and theoretical study. *Chem. Eur. J.* **2020**, *26*, 16530–16540. [[CrossRef](#)]
133. Bellomo, C.; Zanetti, D.; Cardano, F.; Sinha, S.; Chaari, M.; Fin, A.; Maranzana, A.; Núñez, R.; Blangetti, M.; Prandi, C. Red light-emitting Carborane-BODIPY dyes: Synthesis and properties of visible-light tuned fluorophores with enhanced boron content. *Dyes Pigm.* **2021**, *194*, 109644. [[CrossRef](#)]
134. Chaari, M.; Kelemen, Z.; Choquesillo-Lazarte, D.; Teixidor, F.; Gaztelumendi, N.; Viñas, C.; Nogués, C.; Núñez, R. Efficient blue light emitting materials based on *m*-carborane-anthracene dyads. Structure, photophysics and bioimaging studies. *Biomater. Sci.* **2019**, *7*, 5324–5337. [[CrossRef](#)] [[PubMed](#)]
135. Ferrer-Ugalde, A.; Sandoval, S.; Reddy Pulagam, K.; Muñoz-Juan, A.; Laromaine, A.; Llop, J.; Tobias, G.; Núñez, R. Radiolabeled cobaltabis(dicarbollide) anion graphene oxide nanocomposites for in vivo bioimaging and boron delivery. *ACS Appl. Nano Mater.* **2021**, *4*, 1613–1625. [[CrossRef](#)]
136. Conway-Kenny, R.; Ferrer-Ugalde, A.; Careta, O.; Cui, X.; Zhao, J.; Nogués, C.; Núñez, R.; Cabrera-González, J.; Draper, S.M. Ru(II) and Ir(III) phenanthroline-based photosensitisers bearing o-carborane: PDT agents with boron carriers for potential BNCT. *Biomater. Sci.* **2021**, *9*, 5691–5702. [[CrossRef](#)] [[PubMed](#)]

Disclaimer/Publisher’s Note: The statements, opinions and data contained in all publications are solely those of the individual author(s) and contributor(s) and not of MDPI and/or the editor(s). MDPI and/or the editor(s) disclaim responsibility for any injury to people or property resulting from any ideas, methods, instructions or products referred to in the content.